ADDIS ABABA UNIVERSITY
SCHOOL OF GRADUATE STUDIES

INVESTIGATION OF THE UPPER CRUST IN THE CENTRAL MAIN ETHIOPIAN RIFT USING GRAVITY METHOD

BY

MEBATSEYON SHAWEL

June, 2009

Addis Ababa

INVESTIGATION OF THE UPPER CRUST IN THE CENTRAL MAIN ETHIOPIAN RIFT USING GRAVITY METHOD

By

Mebatseyon Shawel

A Thesis

submitted in partial fulfillment

of the requirements for the degree of

Master of Science in Exploration Geophysics

to the School of Graduate Studies

Addis Ababa University

June, 2009

Addis Ababa University

School of Graduate Studies

INVESTIGATION OF THE UPPER CRUST IN THE CENTRAL MAIN ETHIOPIAN RIFT USING GRAVITY METHOD

By

Mebatseyon Shawel

(Department of Earth Sciences)

Approved by Board of Examiners

Dr. Tilahun Mammo _____

Advisor

Dr. Tigistu Haile _____

Examiner

Ato Befekadu Oluma _____

Examiner

Dr. Balemual Atnafu _____

Department head

DEDICATION

I dedicate this work to God my provider for his help in all my weaknesses.

ACKNOWLEDGEMENTS

I would like to express my sincere gratitude and appreciation to Dr. Tilahun Mammo, my advisor, who made this thesis possible and has always lent support, understanding, and above all patience during preparation of this thesis.

My deepest thanks to my father, Mother, brother and sister for their encouragement, support, and prayers throughout my study, and for all the useful advice that helped me obtain this achievement.

Thumbs-up gratitude, to all my family, fellow students and friends for their moral support.

ABSTRACT

The Main Ethiopian Rift (MER) connects the Afar depression, in the north, and the Kenyan rift in the south. It is divided geographically into three sectors: the northern, central and southern sectors. In this project a possible density model for the upper crust of the central MER is presented using gravity data collected by the Ethiopian Institute of Geological surveys (EIGS). The gravity data are tied to the International Gravity Standardization Net, 1971 (IGSN 71) and all standard corrections including the terrain correction are performed. The model, constrained by geophysical and geological data, reveals the presence of the Mesozoic sequence lying between the Cenozoic volcanic rocks and the Precambrian basement rocks. Moreover, combined filtering and horizontal gradient methods performed on the complete Bouguer gravity anomaly have outlined the rim of a large caldera buried under the central sector of the MER.

TABLE OF CONTENT

LIST OF FIGURES

CHAPTER ONE

1. INTRODUCTION

1.1. BACKGROUND

The Ethiopian Rift (ER) is the northern segment of the East African Rift system (EARS) separating the Somalia and Nubian plates. It extends south-southwest from Lake Abbe triple junction, in Afar, to the Lake Turkana region (Korme et al., 1997). This graben is about 800 km long and up to 60-80 km wide. The borders of the rift form flat shoulders about 2200 m high, from which volcanic edifices such as the Chike, the Chilalo and the Kaka attain altitudes of up to 4200 m (Figure 1). The rift floor, on the other hand, rises in a rather irregular fashion from the lake Turkana region to a maximum height of over 1800m a.s.l at the water shed north of Ziway, and descends northwards in much more regular fashion into Afar depression, where it lies below sea level.

The Main Ethiopian rift (MER) connects the Afar depression, in the north, and the Kenyan rift in the south. It is a symmetrical graben with steep border faults dividing the thousand km wide uplifted Ethiopian volcanic province asymmetrically into the northwest and southeast plateaus (Woldegabriel et al., 1990). Volcanic sequences are more voluminous and widespread on the northwest plateau than on the opposite side. The MER is divided geographically into three sectors: the northern, central and southern sectors.

Geologic sections exposed along most of the rift margins are dominated by Tertiary volcanic rocks except for a few locations where crystalline basement is unconformably overlain by Mesozoic sedimentary and/or Tertiary volcanic rocks (Woldegabriel et al., 1990). Such pre Tertiary rocks covered by Tertiary basalt are also present along the eastern, western and southern Afar margins. The rift floor is mainly covered by quaternary basaltic, trachytic and rhyolitic lavas, pyroclastic flows and fall deposits, and volcaniclastic sediments and is obliquely cut by a major NNE-SSW striking active fault system known as the Wonji Fault Belt (WFB). The rift floor also comprises calderas which are generally elliptical in plan view, with the long axes ranging in length between 2 and 17 km.

Models developed based on surface geologic data or on conceptual rifting process commonly suggested that rift propagation in the MER progressed northward (Keranen and Klemperer, 2007; and references therein), although the evolution is not well understood.

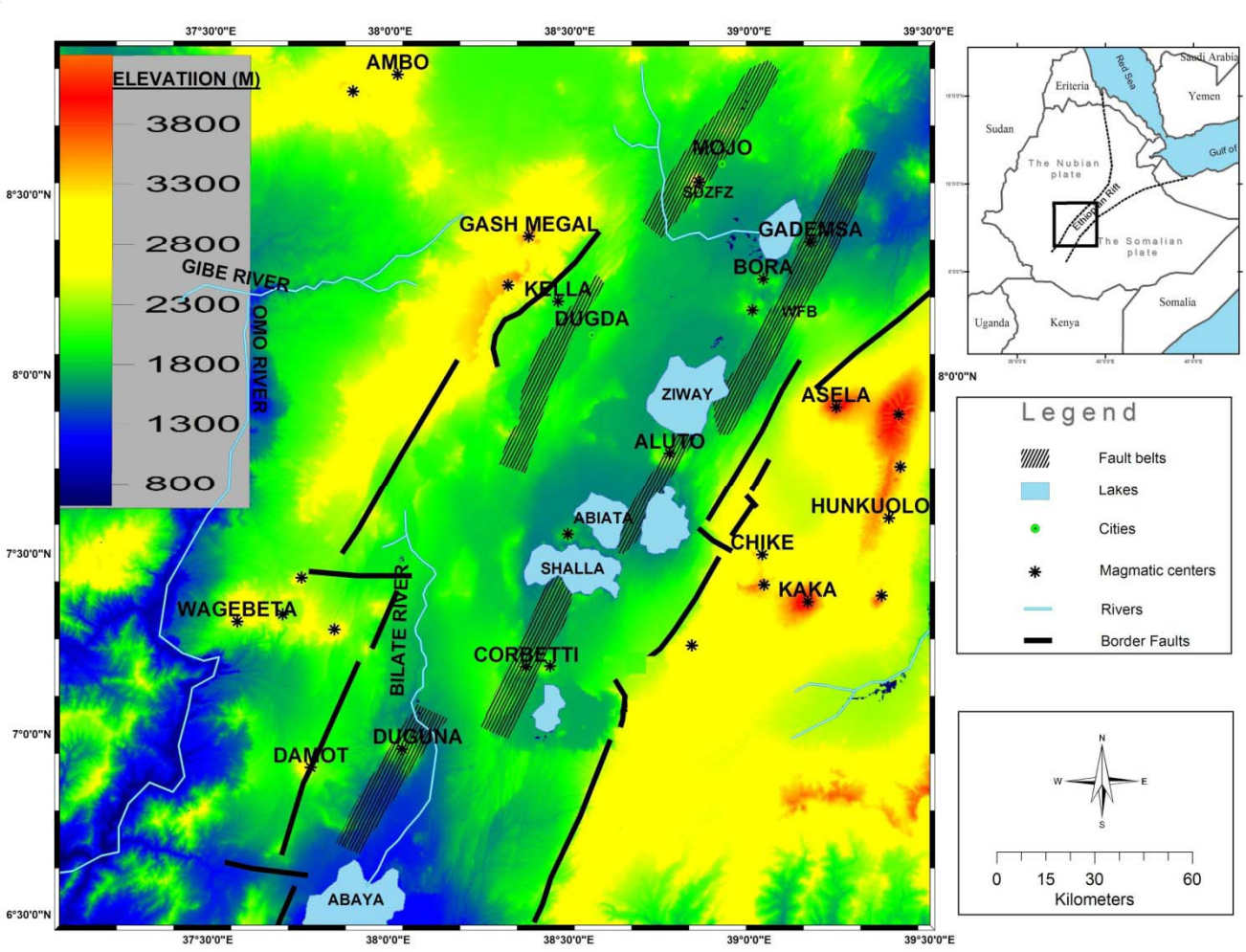

Figure 1.1. Location map of the study area. Color-coded Shuttle Radar Topography Mission digital elevation model (DEM) with 90m resolution overlain by major tectonic structures and magmatic centers.

Alternative hypotheses, such as a proposed model of rift initiation via dike emplacement from beneath Afar or a model of northward plate motion over a stationary hotspot, imply southward propagation. Bonini et al., 2005 in Keranen and Klemperer, 2007 suggested a heterogeneous time-space propagation, with initial extension in the Southern MER propagating northward until 11 Ma, while the southward propagation of the Northern MER from Afar took place after 11 Ma, and formation of the central MER since 5-6 Ma.

In the past much of the research work in the MER concentrated on understanding mechanism of formation and propagation of the rift and its relation to the extensive

volcanic rocks in the region. Gravity surveys were usually used for qualitative interpretations of the relative positive Bouguer anomaly and its relation to intrusions along the rift axis. Quantitative interpretations were employed to show the relative arrangement, density and depth of large scale geologic phenomena like intrusions. In this project, the focus is on determining a density model for the upper crust in the central MER. This will have scientific and economic implications; the Mesozoic sedimentary sequence, if present, being set up in favorable conditions in terms of host rocks, reservoir rocks, overlying load and structural traps has the potential to be an important source of oil and gas, and hence encouraging further investigation for oil and gas in the Main Ethiopian rift. The data and interpreted sections are also helpful in laying down the ground for future scientific research activities regarding the Mesozoic sequence in MER.

1.2. OBJECTIVES

General objective of the study is to investigate geology of the upper crust in the central sector of the Main Ethiopian rift using gravity method.

The specific objectives include:

- Verifying the presence of the Mesozoic sedimentary layer in the CMER on the scale of study,
- Determining thickness of layers composing the upper crust, and
- Outlining related tectonic structures.

1.3. METHODOLOGY

The approach involves using measured Earth's gravitational field to map subsurface variations in density, since this variation is related to change in lithology. There are other aspects that affect the force of attraction experienced by the fixed mass, but these effects can be determined and removed so that the residual variations can be related to the subsurface distribution of density.

The main task in this project is data processing and interpretation. These will be done in steps; first point gravity data will be reduced to datum, following this various filtering and enhancement techniques including wavelength filtering, derivative techniques and others will be used to suppress noise and to better interpret anomalies of interest. Finally the data will be modeled along selected traverses and geologically compatible sections drawn. Other forms of data primarily geophysical model from seismic refraction survey, available borehole data and geological cross sections will be used to constrain the gravity model.

1.4. PREVIOUS WORKS

A number of geophysical studies have been reported in the EARS since the work of Bullard (1936) by several researchers, which substantially improved our understanding of the crustal structure beneath the East African rift system. Recent studies include teleseismic delay times, gravity and electrical conductivities (Tessema and Antoine, 2004). To mention some, Mahatsente et al., 1999 worked out a three-dimensional interpretation of the Bouguer anomaly map of the MER and showed that the inferred zone of intrusion coincides with the maximum gravity anomaly of the rift floor. Later, by compiling new and existing gravity data Tessema and Antoine, 2004 assessed the nature of the crust beneath the East African rift system. The results of the 3D model revealed northward thinning of the crust and the regular patterns in the residual Bouguer anomaly were interpreted as zones of crustal thinning through which relatively dense materials have intruded the crust. Keranen and Klemperer, 2007 used seismic, gravity and geologic data to study the lithospheric structure in the MER and concluded that the sectorization seen at the surface is fundamental, extends through the crust into the upper mantle, and reflects the nature of the processes that have created the rift. They also interpreted the Yerer-Tullu Wellel volcanotectonic Lineament as an integral part of the Main Ethiopian Rift evolution.

CHAPTER TWO

2. GEOLOGY

2.1 REGIONAL GEOLOGIC SETTING

I. The Precambrian shield in Ethiopia occupies a unique position situated between the predominantly gneissic rocks of the Mozambique belt, to the south in eastern and southern Africa, and the volcano-sedimentary plutonic complexes along strike to the north bordering the Red sea (Tefera et al, 1996). The Mozambique belt has been recognized as polycyclic complex comprising units of highly varying lithology, metamorphic grade and age. It contains Gneisses of at least Early Proterozoic and possibly Archean age. On the other hand, studies have shown that the Red Sea region consists of at least five northerly trending volcano-sedimentary belts, largely separated by strips that contain ophiolitic rocks. These are now generally accepted to be accreted arc complexes of Pan-African age (ca. 1000-450Ma) with intervening remnants of dismembered oceanic crust.

II. In the Mesozoic era two major transgression-regression cycles took place; the first transgression started in the early Jurassic from the Ogaden region towards North West and reached its maximum extent in Kimmeridgian (Tefera et al, 1996). During this time Adigrat, Hamanilei, Abay and the Urandab and Antalo formations were deposited when the transgressive sea appears to have reached as far west as 36^0E longitude. Regression of the sea at the end of Jurassic resulted in deposition of the Agula formation and the Gabredare formation. The second major transgression event took place in Aptian to Turonian depositing Mustahil, Ferfer and Belet Uen formations and this was followed by the second regression event in the late Cretaceous which resulted in depositing continental sediments of the Amba Aradom formation.

III. The Ethiopian volcanic terrain was constructed by several episodes of eruptions in the Cenozoic representing diverse petrologic compositions. Volcanism and rifting in major continental rifts generally are either attributed to, or cause, asthenospheric upwelling that induces melting within the underlying sub-continental mantle (Woldegabriel et.al., 1990). Chemical and isotopic data suggest that the mantle below the MER was heterogeneous

and that melting involved enriched and depleted mantle reservoirs and ocean-island basalt (OIB) type mantle sources. Geographic distribution and compositional diversity among volcanic units of the Ethiopian volcanic province indicate that there has been a relationship between magma composition and rifting processes. Volcanic rocks from the MER, Afar, and the plateaus on either side of the rift generally straddle the tholeiitic-alkalic boundary in an alkalies-silica diagram (Woldegabriel et al., 1990; and references therein). The compositional similarity between Teritary transitional basalt from the plateaus and the rifts has been attributed to intensity of tensional tectonic movements during volcanism where basalts of more tholeiitic affinity were associated with intense volcanotectonic activities. During the initial stages of volcanism and rifting, lithospheric melting predominated and crustal contamination was significant and led to transitional basalt with more alkalic character. With time, depleted asthenospheric mantle became an important component, initially as an end member in mantle mixing, and eventually as the dominant mantle reservoir in more attenuated areas(for example, axial zone of MER, Afar) and led to a more tholeiitic transitional basalt.

2.2. GEOLOGICAL UNITS IN THE CENTRAL MAIN ETHIOPIAN RIFT (CMER)

2.2.1 Precambrian rocks

The arcuate western rift escarpment at Guraghe exposes a sliver of the crystalline basement. The basement is represented by an altered Biotite Gneiss intruded by swarms of north west- trending quartzofeldspathic Pegmatites (Woldegabriel et al., 1990). Radiometric dates on the crystalline basement elsewhere in Ethiopia range from 976-370Ma.

2.2.2 Mesozoic Sedimentary rocks

This sequence is found unconformably overlying the crystalline basement at the Guraghe escarpment. Compared to a typical total thickness of more than 1000m in Abay, the sequence at Guraghe is much thinner; 150m of early Jurassic Adigrat sandstone, 20m of variegated shale and 30m of Jurassic Antalo limestone (Woldegabriel et al., 1990). The sequence at Guraghe does not include the Cretaceous strata present elsewhere in the platform Mesozoic sequence of Ethiopia due to either non-deposition or erosion.

2.2.3 Cenozoic rocks

Because volcanic and interbedded sedimentary rocks are likely to be diverse and locally distinct in a rift setting, lithostratigraphy is not an appropriate stratigraphic framework for such a large region (Woldegabriel et al., 1990) and because it is possible to recognize region wide distinct periods of volcanism and interspersed hiatuses from the K/Ar dating, rocks erupted in each period are defined by the K/Ar geochronology as an individual chronozone. Furthermore, within the central sector each of these chronozones corresponds at least in a limited way to a distinguishable volcanic petrology, and so the chronozones are partly specified petrologically.

2.2.3.1. Kella basalts (26-32 Ma)

The oldest volcanic rocks in the CMER outcrop at Agere Selam and kella (Woldegabriel et al., 1990). At Kella, fine grained Oligocene basaltic flows are found overlain by fluvial strata. These 40-60m thick lavas are exposed along fault controlled stream cuts transverse to the rift margin. The unit is also found at Ambo lineament unconfrmably overlying the cretaceous upper Sandstone. The Agere Selam section, which is the eastern rift margin, exposes different rocks. The basal porphyritic olivine-basalt yield an age of 28.9 m.y., the middle of the section contains a Rhyolite dated 31Ma capped by 29.7 m.y. old Mugearite lava. These Oligocene rocks are dominated by Basalt with localized Rhyolite and sedimentary strata. They are generally aphyric, compact rocks, in places showing stratification and contain rare interbedded basic tuffs. The basalts show a distinctive tholeiitic nature with transitions to mildly alkaline varieties. Time correlative lavas are widespread in the Blue Nile (Abbay) and Mugher Rivers of the northwest Ethiopian plateau north of Ambo, the broadly rifted zone of southwest Ethiopia, the Bale Mountains southeast of the central sector, and the margins of the southern sector of the MER.

2.2.3.2. Shebele Trachyte (12-17Ma)

These are exposed in deep river canyons of the Wabi Shebele and Omo Rivers on either side of the rift (Woldegabriel et al., 1990). The Wabi Shebele River flows into a deep canyon about 50-60km east of the Munesa-Asela. The exposed section on the walls of the canyon consist of more than 150m of Agglomerate and bedded volcaniclastic strata

overlain by 25m thick, mid-Miocene, basic lava flows. The lavas are capped by at least four mid-Miocene pyroclastic units represented at the base by a scoriaceous welded tuff which is 16.6 Ma. In the same section two bedded pumice fall deposits covered by lithic-rich welded tuff yield a stratigraphically inconsistent age of 14Ma. The pyroclastic rocks are covered by a 50m thick Trachyte dated at 16.1 Ma.

Mount Chike is the only one of the numerous rift shoulder volcanoes that is made up of the group. The age of the Wabi Shebele mid-Miocene lavas and pyroclastic rocks is similar to, but somewhat older than, the phonolitic lavas investigated from Mount Chike. The coarse nature of the pyroclastic rocks, their absence farther downstream, and the upstream increase in thickness of the 16 Ma Trachytic lava indicates a close by source compatible with their having been erupted eastward from Mount Chike. Similarly, the Omo river canyon west of Damot exposes more than 1.2 km of volcanic rocks and sedimentary strata in two dissected fault scarps. The volcanic rocks along the eastern canyon wall are dominated by mid-Miocene rhyolite, trachyte, basalt and pumiceous pyroclastic flows that are unconformably overlain by Pliocene rocks.

This group in general is of mid Miocene age dominated by undersaturated intermediate and acidic volcanic rocks and consists of Basalt, Trachyte, Phonolite, Rhyolite, and intercalated volcaniclastic strata. Time-correlative basalt, Trachyte, Phonolite, and Rhyolite have been reported from the rift margins of the northern and southern sectors of the MER, the broad rift zone of southwest Ethiopia, and the Afar region.

2.2.3.3. Guraghe Basalt (8.3-10.6 Ma)

Late Miocene basalt and subordinate silicic flows are present at Awasa, Guraghe, and the Omo River canyon. There are at least 14 thick, generally aphyric basalt flows and intercalated vitric ash exposed at the main Guraghe section, yielding an age (10.6-9.1 m.y.) for the basalt and top flows of the section (Woldegabriel et al., 1990). Some lavas are represented by Scoriaceous horizons with no apparent erosional surface between the lavas, implying rapid extrusion. Total thickness of the section is approximated to be 2850m. The Gash Megal topographic high along the western rift shoulder, west of Guraghe, is a late Miocene Rhyolite overlying time correlative basaltic flows (10 Ma.).

The eastern wall of the Awasa caldera asymmetrically overlaps the eastern rift margin. There, a 500m thick composite column from two adjacent sections (2km apart) consists of

Miocene (9.8-9.7Ma.) aphanitic Mugerite and a welded vitric tuff exposed in the basal part of the western section, their thickness is ~70-80m. In the eastern Omo River canyon wall there is ~100m thick exposure; here the 10.6m.y. old basalt is underlain by several undated basalt flows and mid-Miocene (15-16.9 Ma) Shebele group rhyolite and trachyte flows. Time-correlative late Miocene rocks are widespread along both rift margins and shoulders of the rift system.

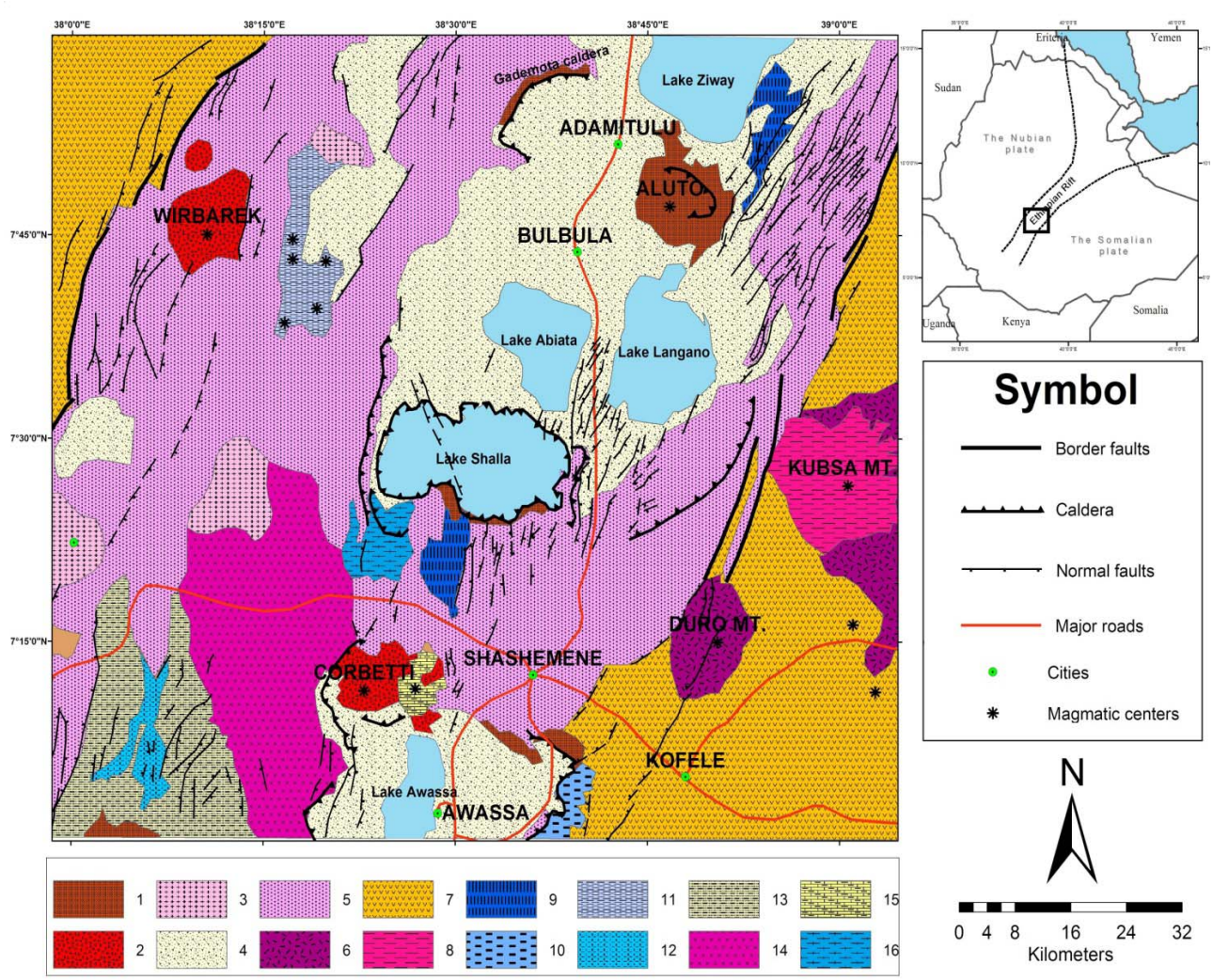

1-Rhyolitic and trachytic lava flows, 2- Pumice and unwelded tuffs, 3- Peralkaline silicics undifferentiated, 4- Lacustrine sediments, silts, clays, diatomites, volcanoclastics and tuffs, 5- Ignimbrites, Tuffs, waterlain Pyroclastics, occasional lacustrine beds, 6- Trachytes, trachybasalts, peralkaline rhyolitic ignimbrites, 7- Nazret Group and Dino formation, 8- Alkaline basalts, 9- Pleistocene basalts, 10- Alkaline basalts, trachytes and peralkaline rhyolitic ignimbrites undifferentiated, 11- Recent and subrecent basalt flows and cones, 12- Ignimbrites, alkaline basalts, trachytes and peralkaline rhyolitic ignimbrites undifferentiated, 13- Volcano-sedimentary rocks: lacustrine, predominantly volcanoclastic sediments, tuffs 14- Coarse unwelded pumiceous pyroclastics, 15- Obsidian and pitchstones, 16- Basaltic hyaloclastites,

Figure 2.1 Geological map of the central Main Ethiopian Rift. Taken from the Ethiopian Institute of Geological surveys (EIGS)

2.2.3.4. Butajira Ignimbrite (3-4.2 Ma)

The early to middle Pliocene epoch (4.2-3 Ma) was characterized by the eruption of voluminous silicic pyroclastic material (from the Awasa caldera, the Wagebeta caldera complex, and a major caldera probably buried beneath the Ziway- Langano- Abiata basin) and by subordinate basaltic flows (Woldegabriel et al., 1990). At the Kella Pliocene basalt flow (4.2-2.5 Ma) and particularly crystal rich welded tuff is found overlying the Oligocene Basalts. It thickness exceeds a total of 400m and from the section a single crystal rich tuff (15-40 volume percent crystal, 3.5 Ma) dominates with a thickness of 200-250m. The top of the section at main Guraghe is capped by 20m thick pliocene welded tuff (3.85 Ma.) This sequence also blankets the Gash Megal with a thickness of 30-40m. The Wagebeta caldera west of the Guraghe, feldspar separate from welded tuff along the eastern wall of the Wagbeta caldera yielded a date of 4.2Ma where as a Rhyolite lava 10 km to the south east is 3.6 m.y. In the geothermal well LA-3 bottomed at 2,143m a thick (>400m) hydrothermally altered crystal rich, welded tuff is found. It is petrographyically and geochemically very similar to the main crystal rich tuff exposed along the Guraghe. The Omo river canyon also exposed ~50m thickness of this group. At Awassa caldera wall this section is exposed unconformably overlying the late Miocene rocks with a thickness of 20-30m Chemical and petrologic data distinguish rhyolitic rocks of the Butajira ignimbrite from those of the quaternary Wonji Group as being calc-alkaline or mildly peralkaline rather than peralkaline. Although the proximal, welded pyroclastic rocks are confined to the MER and its immediate shoulders, primary and reworked distal air-fall units may be in northern Kenya, the Afar, and the Gulf of Aden. Voluminous time-correlative units are present in the northern sector.

2.2.3.5. Chilalo Trachyte (1.6-3.5 Ma)

This middle to upper Pliocene stratigraphic unit is a modification of the Chilalo-Badda Trachyte so as to include the products of the Pliocene centers of the eastern and western shoulder of the rift and compositionally correlative units from the Awasa caldera (Woldegabriel et al., 1990). This unit is found at a depth of 690m at the geothermal well

LA-3 on the Aluto caldera having a thickness of ~900m. The Munesa section, at the eastern escarpment, on the other hand, exposes 2.83-2.95 Ma vitrophyric tuff (1-2m thick). Locally, 2m basalt dated 2.54 Ma and 3.48-3.17 Ma tuff are present along north-northeast trending horsts in front of, and parallel to, the rift margin at Munesa. In the canyon section at Wabi Shebele, the top of the section consists of three basaltic units dated between 2.82-.286 Ma and in Agere Selam these late Pliocene units, crystal rich welded tuff are found unconformably overlying the Oligocene rocks. The eastern topographic wall of the Awasa and rocks around the Awasa-Corbetti caldera are similar in lithology and age to those observed in the Bilate River drainage basin except for a 2.5 m.y. old rhyolite from a horst 5km south of the Awasa caldera margin.

This unit in general includes trachyte, silicic rocks, and basalt that overlie units of either the Shebele Trachyte or the Buajira Ignimbrite. Outside the central sector, time correlative units are confined totally to the rift floor.

2.2.3.6. The Wonji group (<1.6 Ma)

This group consists of diverse quaternary lava, pyroclastic rocks, and volcaniclatic strata (<1.6 Ma) that are generally confined to the Wonji fault belt along the entire MER (Woldegabriel et al., 1990). The Wonji fault belt (WFB) has peralkaline silicic centers along it. The Aluto volcanic center rising more than 600m from the surrounding floor is one example. Two samples from the bases of the northwestern and southeastern slopes of the Aluto are 0.042 m.y. and 0.078 m.y. old. Likewise, the wall of the Awasa caldera exposes several welded-tuff and ash flows bracketed between 1.85-1.1 m.y. in age and about 15km farther south, the rift margin is dominated by basaltic flows that are capped by the 1.1m.y.-old welded tuff. Also included in the chronozone are the young flood basalts from the Silti - Debre Zeit and the 0.68 m.y. old flood basalt in the Ambo area. Outside the study area, the Tepi Basalts of southwest Ethiopia and the Batu Trachyte of the Bale mountains erupted contemporaneously with the Wonji group, as well as comparable units of the rift floor elsewhere along the MER and the Afar.

2.2.4. Quaternary Sediments

Lacustrine sediments composed of sand, clay and diatomite were deposited in the rift floor, during the pluvial periods (period of heavy rainfall between 1 and 0.01 million years) in Pleistocene to Holocene period. The lacustrine sediments are the results of drying up of a

big lake, which in the past occupied the floor of the rift valley. Lake Ziway, Langano, Abijata, and Shalla are in fact the remnants of that ancient large water basin (Mohr, 1971). The thickness of sediments on the floor of lakes basin is not accurately known. Sediments are probably thick in tectonic troughs, which correspond in part to the topographic lows occupied by lakes. Variable sediment thickness occurs, ranging from about 40m in Bulbula River, and 50m in Boru and Meki Rivers. Alluvial deposits composed of silt, sands and gravel occur along the foot of the rift escarpments and the lower reach of rivers such as Meki and Bulbula. In the Ethiopian rift system, Quaternary lavas and pyrocalstic deposits are very frequently interbedded with these sediments.

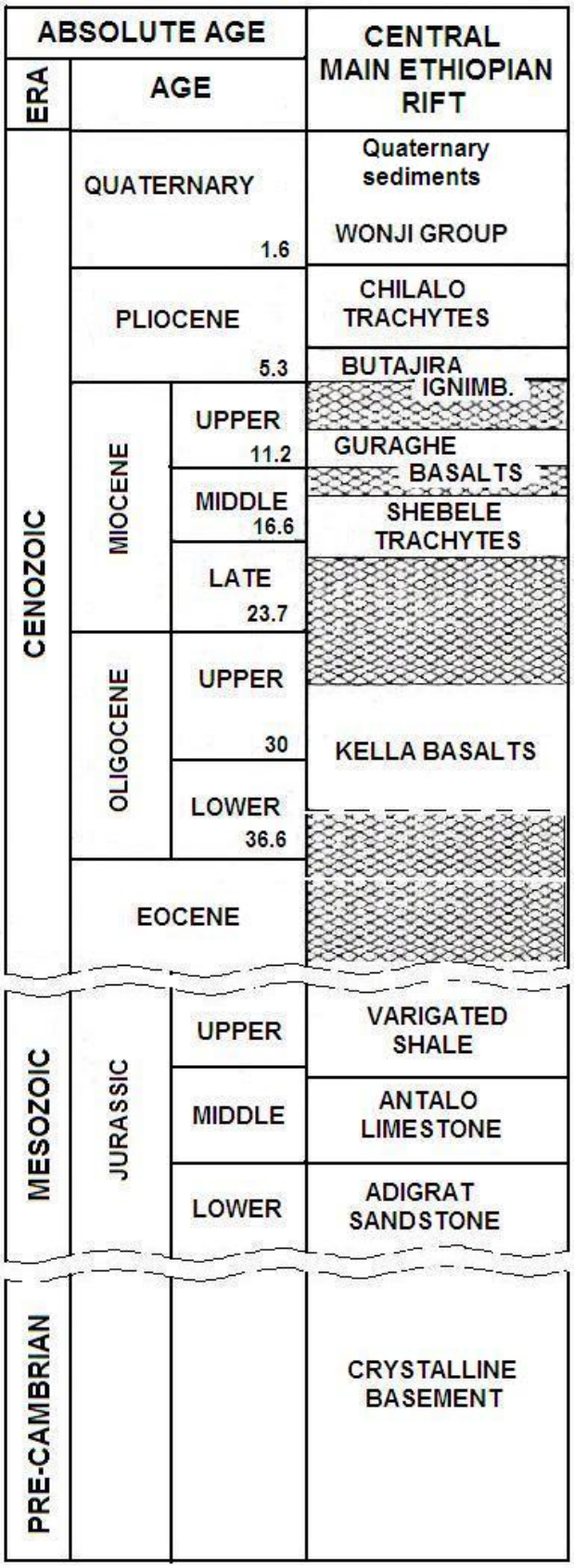

Figure 2.2 Chronostratigraphic column of the central Main Ethiopian rift (modified after Woldegabriel et.al, 1990).

2.3. STRUCTURAL RELATIONSHIPS IN THE CENTRAL MAIN ETHIOPIAN RIFT

The central sector of the MER is a symmetrical rift, mostly characterized by well-defined rift margins having variable throws along the strike of the boundary faults. These margins are marked by high-angle normal faults with large throws that comprise several step-faulted blocks. The faulted margins show right-angled spurs and re-entrants similar to those documented in the broad rift zone of southwest Ethiopia (Woldegabriel et.al., 1990 and references there in). At places, the rift escarpments adjacent to the quaternary silicic centers, located along the rift axis, are generally subdued in part due to pyroclastic accumulation along the margins. Thus, only minimum estimates are available on throws along the normal faults estimated from the height of the fault scarps.

Below the rift structures and their temporal and spatial relationships with the various volcanic rocks are described for the Guraghe-Wabi Sheble River Rift profile (A-A') (Figure 2.3) according to Woldegabriel et.al., 1990 and the corresponding cross section highlighting the structure and physiographic features of the rift flanks, margins, and the floor is given.

At the Guraghe section, more than 1.5km thick flood basalt is exposed by several major step-faults that strike north-northeast and, in turn, are cut by northwest to north-northwest striking transverse faults. The truncation of most of the rift-oriented fault blocks topographically down from, and east of, the main Guraghe escarpment by these transverse faults has resulted in the blocks having a pattern of serrated edges and re-entrants. Overall, the main rift margin at Guraghe seems to have been displaced westward as a net effect of this transverse faulting. Cumulative throw along step faults is at least more than 1.5 Km, considering that the adjacent marginal graben of the rift floor is filled by an unknown thickness of pyroclastic and volcaniclastic rocks that are capped by quaternary basalt.

Because of the complex structural relationships, the evolution of the Guraghe-kella scarp undoubtedly has been complex and has involved a history of tectonic inversion in which originally down dropped blocks have been subsequently elevated. The pre-Tertiary rocks at Guraghe are cut into four tilted individual blocks by west-northwest trending normal cross –faults that are downthrown to the northeast. Now structurally low, the block of pre-Tertiary rocks was probably subjected to a long period of uplift and erosion, because the

more than 200-m thick Cretaceous upper Sandstone (Ambo-Blue Nile or Abbay River gorge), which unconformably underlies the Kella Basalt at Ambo 100 km to the north, is absent in the Guraghe area. Moreover, Oligocene and Miocene lavas of the Kella and Guraghe Basalts are not observed on top of these older rocks. Instead, the Kella Basalt and overlying organic rich fluvial strata devoid of clasts from either the Oligocene or Miocene basalts appear to lap against both flanks of the pre-Tertiary structural blocks. The absence of remnants of the late Miocene basalts flows (Guraghe Basalt) on top of the older rocks (that is pre-Tertiary and mid-Oligocene rocks) suggests that the voluminous fissural eruption of these lavas 11.9 m.y. ago was confined to a graben or down faulted block west of the uplifted horst. This thick(>800m), horizontally layered, basalt sequence was uplifted to form the main rift margin before 8.3 m.y. old, as indicated by containment of westward-tilted 8.3 Ma old, glassy welded tuff that thickens against the main Guraghe escarpment.

After the formation of the main Guraghe escarpment, the previously uplifted fault blocks containing the pre-Tertiary rocks and the Oligocene Kella Basalt dropped. As a result, fault terraces along edges of the block of pre-Tertiary rocks were partially covered by early Pliocene basalt which crops out alongside the pre-Tertiary rocks north of Kella. All of the marginal fault blocks in the Kella area were completely buried in the Pliocene epoch by voluminous welded tuff of the Butajira Ignimbrite. South of Kella, most of these pyroclastic rocks were topographically confined to the base of , and in front of, the main Guraghe scarp covering the 8.3 m.y. old, glassy welded tuff. The total thickness of Pliocene welded tuff exposed along fault blocks in front of the main Guraghe rift margins far exceeds the <40m deposited on the rift shoulder. During the late Pliocene epoch, north-northeast-striking faults exposed the pre-Tertiary rocks again. These rift-oriented faults are cut by quaternary cross-faults that displace 0.1 Ma basalt flows. The interpretation that block faulting controlled the distribution of the Guraghe basalt flows west of the pre-Tertiary block sets 11Ma as a minimum date for the formation of the rift margin. If the flow distribution of the Oligocene basalt on the flanks of the pre-Tertiary rocks is an original feature and not due to erosion, then uplift and faulting possibly occurred as far back as Oligocene time. As mentioned, the anomalously thin Mesozoic sequence of Guraghe possibly reflects a doming stage in the Mesozoic that preceded Tertiary volcanism and rifting.

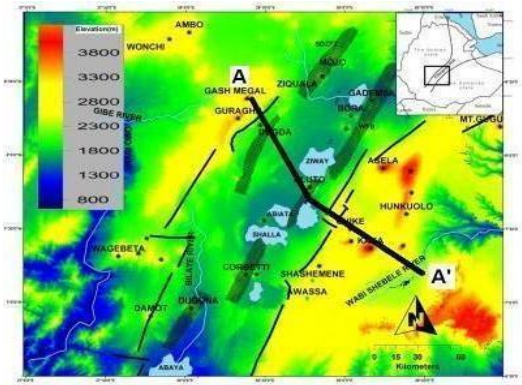

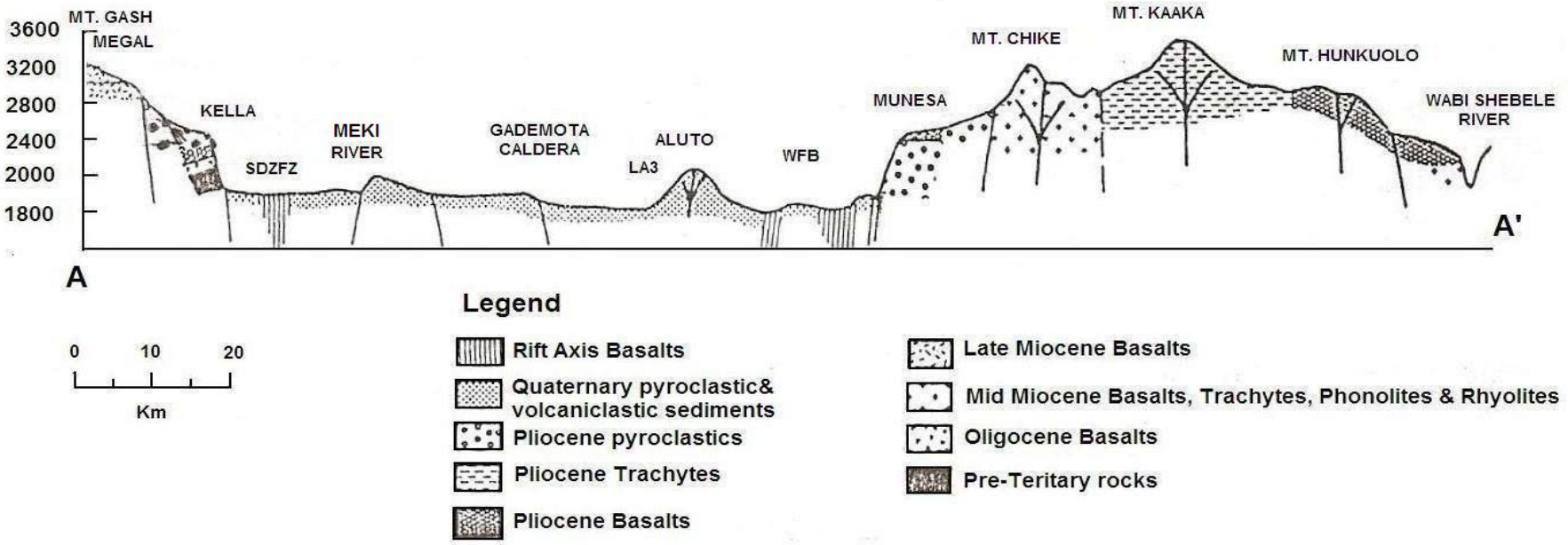

Fig.2.3. Simplified geologic section across the central sector of the Main Ethiopian Rift and adjacent plateaus (A-A'); vertical exaggerations, 12.5X. Elevations in meters aboove sea level, Map shows locations of cross section. Taken from Woldegabriel and others, 1990.

In the northern sector of the MER (Addis Ababa area), evidence for major rift faulting in the late Miocene epoch has been documented and is compatible to that in the central sector. Upper Miocene basalt and Pliocene rocks of the rift floor banked against lower Miocene silicic and mafic rocks of the western rift margin.

The rift floor between Guraghe and Munesa is characterized by two north- northeast trending marginal grabens that are marked by swarms of closely spaced normal faults and associated volcanic flows of the quaternary Wonji Group. The Silti-Debre Zeit fault zone of the western marginal graben is more than 100 km long and 2-5 km wide and converges at its southern end with the medially located Wonji fault belt and young volcaniclastic strata. The Wonji fault belt is the single through going medial volcano-tectonic axis of the MER except in the northern part of the central sector, where it forms the 5-10 km wide eastern marginal graben. In central sector, the fault belt is right laterally offset into four *en echelon* rift-axis segments: Gadamsa-East Ziway, Ziway-Shala, Shala-Awasa, and the Duguna-Abaya zones. Faulting and fissural basalt flows along the belt are more intense than along the Silti-Debre Zeit fault zone. A major cross-fault south of the Aluto center crosscuts north-northeast striking normal faults in the rift floor and extends to, and offsets, the eastern rift margin, forming a right-angled spur along the margin south of Munesa. The interpretation of the presence of the Musesa Crystal Tuff in the base of Geothermal well LA3 inside the Aluto caldera indicates that more than 2 km of vertical displacement between the top parts of the crystal tuff at Munesa (2400m elevation) and in the drill hole (322m elevation) has occurred since mid-Pliocene time. Unlike elsewhere along the MER, faulting on the floor of the northern part of the central sector is progressively younger toward the margins.

Continuing eastward from the rift floor on the cross section of Figure 2.3, the eastern rift shoulder is a broad uplifted plateau of Plio-Pleistocene volcanic rocks, consisting of several trachyte centers and the 70 km long Galama volcanic range, which is related to a structural control by a major line of Precambrian crustal weakness. The north-northeast striking boundary fault of the eastern margin between Munesa and Asela is cut by short oblique faults (north-northwest striking), resulting in serrated edges and open fissures. North-northeast striking open fissures more than 50m deep and 5-30m wide offset 0.3 m.y. old welded tuff north of Munesa. Like the western escarpment, the eastern escarpment had fully formed along the general direction of the present day boundary by Pliocene time,

resulting in a symmetrical rift as confirmed by the total containment of the more that 300m thick,3.5 m.y. old, Munesa crystal Tuff to the rift floor and margin blocks in the northern half of the central sector. Its total absence in the Wabi Shebele River canyon, 50 km east of the rift escarpment, is attributed to the presence of a high rift wall already existent prior to its eruption. This suggestion is further supported by the banking of Butajira Ignimbrite units against the mid-Miocene Chike phonolite center, and the containment of Chilalo Trachyte units against older rocks of the same chronozone at the northern base of Mount Chilalo. As the rift wall at some places is fully composed of the Munesa Crystal Tuff, the pre-existing eastern rift margin in the northern half of the central sector was buried by this major eruption. Intense down faulting along the buried fault after the eruption of the Munesa tuff must have subsequently re-established the escarpment in the late Pliocene slightly inward from the pre-existing escarpment, thus exposing the full thickness of the Munesa Crystal Tuff.

CHAPTER THREE

3. THEORY OF GRAVITY METHOD

In 1687, Isaac Newton came forth with the Universal Law of Gravitation. Newton's law is a mathematical description of one of the most fundamental phenomena of nature. This law states that each particle of matter in the universe attracts all others with a force directly proportional to its mass and inversely proportional to the square of its distance of separation (Telford et. al., 1976). In Cartesian coordinates, the mutual force between a particle of mass m centered at point Q = (x', y', z') and a particle of mass m_0 at P = (x,y,z) is given by:

$$F = \gamma \frac{m m_0}{r^2} \qquad (3.1)$$

where

$$r = [(x-x')^2 + (y-y')^2 + (z-z')^2]^{1/2}$$

and γ is Newton's gravitational constant. Allowing the mass m_0 to be a test particle with unit magnitude, then dividing the force of gravity by m_0 results in the gravitational attraction produced by mass m at the location of the test particle:

$$g(p) = -\gamma \frac{m}{r^2} \hat{r} \qquad (3.2)$$

where $\hat{r}$ is a unit vector directed from the mass m to the observation point P. This value is negative because $\hat{r}$ is directed from the source to the observation point, opposite in sense to the gravitational attraction.

3.1 GRAVITATIONAL POTENTIAL

Gravitational fields are conservative; that is, the work done in moving a mass in a gravitational field is independent of the path traversed and depends only on the end points. Hence, gravitational force giving rise to conservative field may be derived from a scalar potential function U(P), also called the three-dimensional potential, by finding the gradient,

$$\nabla U(P) = -\frac{F}{m_0} = -g(P) \tag{3.3}$$

Alternatively, we can solve this equation for the gravitational potential in the spherical coordinate system, in the form

$$U(P) = U(r, \theta, \phi) = \int_{\infty}^{r} (\nabla U) \cdot dr \tag{3.4}$$

$$= -\int_{\infty}^{r} g \cdot dr \tag{3.5}$$

which is a statement of the work done in moving a unit mass from infinity, by any path, to point distant *r* units from the point mass producing the gravitational field. Using equation (3.2), we get

$$U(P) = -\gamma \int_{\infty}^{r} \left(\frac{m}{r^2}\right) dr = \gamma \frac{m}{r} \tag{3.6}$$

It is often simpler to solve gravity problems by calculating the scalar potential U rather than the vector g and then to obtain g from equation (3.3).

Considering a three-dimensional mass of arbitrary shape, the potential and acceleration of gravity at a point outside the mass can be found by dividing the mass into small elements and integrating to get the total effect. From equation (2.6), the potential due to an element of mass *dm* at the point Q = (x', y', z') a distance *r* from P(0,0,0) is

$$dU = \frac{\gamma dm}{r} = \gamma \rho \, dx \, dy \frac{dz}{r} \tag{3.7}$$

Where $\rho(x, y, z)$ is the density, and $r^2 = x^2 + y^2 + z^2$. Then the potential of the total mass m is

$$U = \gamma \iiint \left(\frac{\rho}{r}\right) dx dy dz \tag{3.8}$$

Because g is the acceleration of gravity in the z direction, and assuming ρ constant,

$$g = -\left(\frac{\partial U}{\partial z}\right) \tag{3.9}$$

$$g = \gamma \rho \iiint \left(\frac{z}{r^3}\right) dx dy dz \tag{3.10}$$

3.2 DERIVATIVES OF THE POTENTIAL

Quantities useful in gravity analysis may be obtained by differentiating the potential in various ways. It is to be noted that $g = -(\partial U / \partial z)$ is the quantity measured by gravimeters. The first vertical derivative of g from eq.(2.10) is

$$\frac{\partial g}{\partial z} = -\frac{\partial^2 U}{\partial z^2} \tag{3.11}$$

$$= \gamma\rho \iiint \left(\frac{1}{r^3} - \frac{3z^2}{r^5}\right) dx dy dz \tag{3.12}$$

which is a measurement of vertical gradient of the gravity field. Similarly the second vertical derivative is

$$\frac{\partial^2 g}{\partial z^2} = 3\gamma\rho \iiint \left(\frac{5z^3}{r^7} - \frac{3z}{r^5}\right) dx dy dz \tag{3.13}$$

Derivatives tend to magnify near surface features by increasing the power of the linear dimension in the denominator (Telford et al., 1990). That is, because the gravity effect varies inversely as the distance squared, the first and second derivatives vary as the inverse of the third and fourth powers, respectively for three dimensional bodies.

By taking the derivatives of *g* in eqn. (3.10) along the *x* and *y* axes, we obtain the components of the horizontal gradient of gravity:

$$\mathbf{U_{xz}} = -\left(\frac{\partial g}{\partial x}\right) \tag{3.14}$$

$$= 3\gamma\rho \iiint \left(\frac{xz}{r^5}\right) dx dy dz \tag{3.15}$$

where U_{xz} indicates derivatives of U.

And similarly for the *y* component U_{yz}. The horizontal gradient can be determined from gravity profiles or map contours as the slope or rate of change of 'g' with horizontal displacement. The horizontal gradient is useful in defining the edges and depths of bodies.

3.3 FIGURE OF THE EARTH

3.3.1 The reference spheroid

If the earth were a perfect fluid with no lateral variations in density, its surface would correspond to an ideal ellipsoid of revolution, the so-called normal spheroid. This would be a level surface, and the direction of gravity everywhere would be perpendicular to the surface. Geodetic measurements have determined the shape of the earth to be nearly spheroidal, bulging at the equator and flattened at the poles with polar flattening $(R_{eq} - R_p)/R_{eq} = 1/298.25$, where R_{eq} and R_p are the Earth's equatorial and polar radii, respectively. Hence, the reference spheroid approximates the mean sea-level surface (geoid), with the land above it removed.

In 1930 the International Union of Geodesy and Geophysics (IUGG) adopted a formula for the theoretical value of gravity '$\mathbf{g}_t$', but this has been superseded by the Geodetic Reference System 1967 (GRS67) where '$\mathbf{g}_t$' is given by:

$$\mathbf{g}_t = 978031.846(1 + 0.005278895 \sin^2\phi + 0.000023462 \sin^4\phi) \text{ mGals} \quad (3.16)$$

ϕ is the angle of latitude.

The first term of the gravity formula is the value of gravity at sea level at the equator. Its value depends both on a systematic adjustment of relative gravity measurements over the earth's surface and on an absolute value of gravity at some one place, to which the relative measurements are referred. Any recognized correction would also apply to the first constant of the gravity formula.

3.3.2 The Geoid

Sea level is influenced by variations in elevation and other lateral density changes. We define mean sea level (the equipotential for the Earth's gravity plus centrifugal effects), called the geoid, as the average sea level over the oceans and over the surface of sea water that would lie in canals if they were cut through the land masses. An ordinary spirit level indicates a surface parallel to the geoid.

The actual level surface is deformed or warped. Evidence for this warping is given by small deviations of the plumb, or vertical, from the direction it would have if it were perpendicular to the normal spheroid. Due to this warping the deviations between the reference spheroid and the Geoid are as much as 100m.We might expect the geoid to be warped upward under the continents because of attracting material above and downward over the ocean basins because of the low density of water. However, deviations from the spheroid do not correlate with the continents or with the lithospheric plates, suggesting that density differences exist below the lithosphere (Telford et al., 1990).

3.4 GRAVITY OF THE EARTH

Because the Earth is not a perfect homogeneous sphere, gravitational acceleration is not constant over the Earth's surface. Its magnitude depends on five factors: latitude, elevation, topography of the surrounding terrain, earth tides and density variations in the subsurface (Telford et al., 1990). Gravity exploration is concerned with anomalies due to the last factor, and these anomalies generally are much smaller than the changes due to latitude and elevation, although larger than the anomalies due to tidal and usually topographic effects. The change in gravity from equatorial to Polar Regions amounts to about 5 Gal and the effect of elevation can be as large as 0.1 Gal, whereas in mineral exploration a large anomaly would be 1 mGal. Thus, variations in 'g' significant in prospecting are small in comparison with magnitude of 'g' and also in comparison with latitude and elevation effects. Nevertheless we can, with good accuracy, remove most of the effects of factors that are not of interest in prospecting.

This section describes the factors that affect gravity exploration and the standard corrections that are applied to remove them.

3.4.1. Gravity Tidal and Drift correction

Tidal effects are external time variations of gravity which result from the variation in the gravitational attraction of the sun and the moon as their positions change with respect to the earth. For certain configurations of the sun and the moon, rotation of the earth produces changes that have maximum amplitude of about 0.3 mgal and occur in a period as short as about 6 hr. The tides consist of a component that peaks approximately twice a day, a component that peaks approximately daily, and longer period components which peak every 14 days as a result of the moon and 6 months as a result of the sun (Nettleton, 1976). In addition, the gravitational attraction which causes tidal effects at sea also cause the solid earth to react in the same way. These solid Earth tides can cause the gravity station to vary in elevation by a few centimeters, thus increasing the distance to the center of the Earth causing a maximum change of 0.3 mGals in a minimum period of 12 hours. In a high precision survey, these tidal variations must be corrected for by reoccupying the base station at an interval less than the period of Earth tides. On the other hand, a phenomenon known as drift occurs in every gravimeter. Drift is defined as the change in the elasticity of the springs over time and is different for every gravimeter.

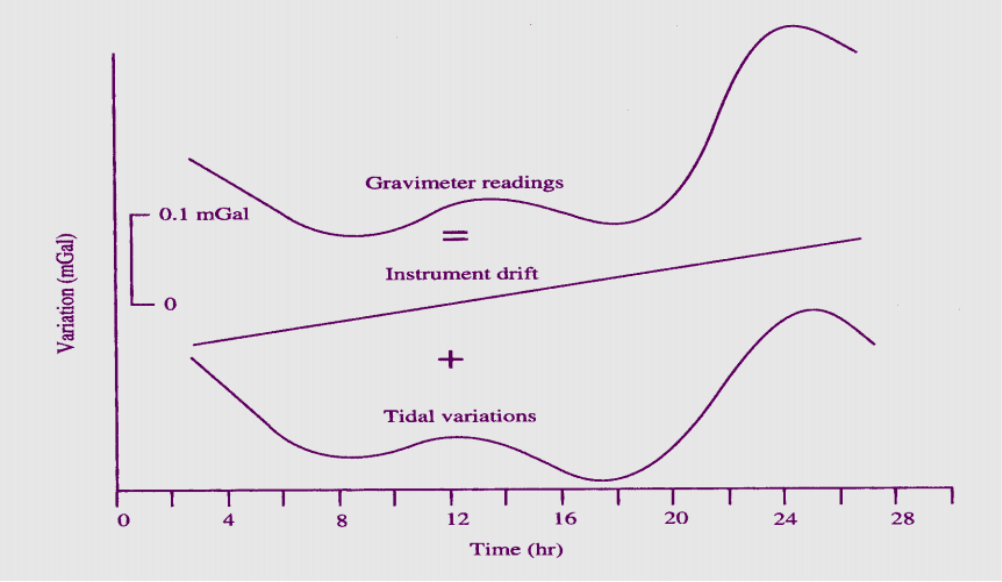

Figure 3.1 Typical gravimeter reading variation curve at a base station which is a combination of instrument drift and earth tidal variations (adopted from Burger, 1992)

Corrections to the observed gravity readings for instrument drift and tidal effects require one to occupy a base station several times during the day of the survey because of their erratic nature. The meter reading is plotted against time and it is assumed that drift and

tidal effects are linear between re-occupations. The correction is then subtracted for each station.

3.4.2. Latitude correction

The equatorial radius of the earth is about 21 km greater than the polar radius and this flattening towards the Polar Regions means that the acceleration of gravity is 5.17 gals greater at the poles than at the equator. The normal northward or southward gravity increase is maximum in middle latitudes amounting to about 0.87 mgals/km (Nettleton, 1976).

The latitude correction takes account of the increase of gravity from equator to pole. Latitude corrections are nearly always based on gravity differences derived directly from the gravity formula. Since modern instruments can be read to a few hundredths of a milligal, it is desirable to attempt to keep the corrections accurate to 0.01 mgal.

3.4.3. Free air correction

Gravity varies with elevation because a point at a higher elevation is farther away from the center of the earth and therefore has lower gravitational acceleration than one at lower elevation. The rate of this normal vertical variation, or the vertical gradient of gravity, can be calculated quite accurately from the gravity formula and the radius of the earth (Nettleton, 1976). This can be shown as:

$$\frac{dg}{dz} = \frac{dg}{dR} = -\frac{2GM}{R^3} = -\frac{2g}{R} \qquad (3.17)$$

If we take for the mean radius of the earth R=6.67x10^8 cm and for the theoretical value of gravity at sea level and at 45^0 latitude g =980.629 gals, then

$$\frac{dg}{dz} = -\frac{2 * 980.629}{6.367 * 10^8} = -0.3086 \frac{mgal}{m}$$

There is a small second order term which is appreciable only at high elevations. This term amounts to only 0.07 mgal for an elevation of 1000 m, about $0.07h^2$, where h is in kilometers. This is nearly always neglected. If a proper correction for elevation effect were not made, a gravity map would be strongly affected by differences in elevation between

different points of measurement. Therefore, a correction for the elevation is always made before mapping gravity measurements made for gravitational prospecting.

The vertical decrease of gravity with increase of elevation is taken care by the free air correction. This variation has a magnitude of 0.3086 mgal/m. The correction can be made to any arbitrary reference or datum level that is convenient.

3.4.4. The Bouguer correction

This correction takes into account the material between the gravity station and the geoid surface. There are three parts to this correction. The first part assumes an infinite horizontal slab of rock of uniform density whose thickness is the elevation difference between the gravity station and the geoid surface. The density is equivalent to the mean density of bedrock found in the region. Generally, for the purpose of comparison to other surveys this density is 2.67 gm/cm^3. Observed gravity readings are increased by the rock mass between the station and the datum, therefore, the Bouguer correction is subtracted when the station is above the geoid surface. The Bouguer correction is:

$$BC = 0.0418\,\rho h \text{ mGal} \qquad (3.18)$$

Where ρ is the density of the slab and h is the thickness of the slab.

The second part of the Bouguer correction adjusts the slab to account for the curvature of the Earth's surface. This modification changes the horizontal slab to a slab with a spherical cap of radius 167 km. The formula for this correction is:

$$CC = \frac{4.462\text{x}10^{-4}h}{0}.3048 - \frac{3.282\text{x}10^{-8}\,h^2}{([0.3048)^2} + \frac{1.27\text{x}10^{-13}\,h^3}{([0.3048)^3} \text{ mGals} \qquad (3.19)$$

The concept of a horizontal infinite slab existing between the station and the datum is not really valid due to local variations around the station in topography. Regions that exist above the Bouguer slab and therefore not accounted for in the Bouguer correction, exert an upward pull at the station thus decreasing the observed gravity reading. It is necessary to add a positive terrain correction to compensate for this upward attraction. Depressional

features are accounted for in the Bouguer slab, however, they do not contain mass. The Bouguer correction therefore overcompensates for these regions and so a positive terrain correction is needed to restore the slab to a flat area. Therefore, for both hills and valleys the terrain correction is added back to the gravity readings. Once corrections have been made to the observed gravity values, the result would reflect the variations of geology within the Earth model. This is called the Complete Bouguer Gravity Anomaly (CBGA) and is represented below:

$$CBGA = g_{observed} - g_{latitude} + FAC - BC + TC - CC \quad (3.20)$$

Where $g_{observed}$ is the observed gravity, $g_{latitude}$ refers to latitude correction, FAC is the free air correction, BC refers to the Bouguer slab correction, TC refers to terrain correction and CC is the curvature correction. CBGA values are the standard for Earth gravity models (Keary et al, 1991).

3.5. GRAVITY DATA REQUIREMENTS

3.5.1. Observations for drift correction

To provide data for the drift and tide corrections, the gravity meter is returned to a reference station at intervals depending on the stability of the meter and the precision expected of the survey. It is not necessary for drift readings to be made at the same station if other points with previously established gravity values are more convenient. The readings can be reduced to what they would have been at a single reference point or base station by properly taking into account the gravity differences between bases. These drift readings impose conditions on the field operations which are often onerous but are necessary. If drift observations are made at intervals of about 2 hr or less and meter performance is good, there is little loss in precision by simple linear interpolation between drift readings (Nettleton, 1976). A curve is plotted of the readings at the base station including those at other based, referred back to the first by the established differences. Readings at other stations are then referred to this curve.

3.5.2. Elevation requirements

The contribution of free air and Bouguer effects causes a change of gravity with elevation. Within the range of usual surface densities, of 2.6 to 1.8, the factor varies from about 0.06 to 0.23 mgal/m. This means that if reduced gravity measurements are to be accurate to 0.1

mgal or less, the relative elevations must be determined to 0.3m or less (Nettleton, 1976). If the ultimate precision of modern gravity meters, about 0.01mgal, is to be retained in the final values, relative elevations must be reliable to about 0.06m.

3.5.3. Position requirements

The required relative precision of station locations (horizontal control) is dictated by the latitude corrections. The horizontal gradient K, or rate of change of gravity with the north-south component of distance, can be derived from the gravity formula.

$$K = \frac{dg}{dx} = \frac{dg}{rd\varphi} \qquad (3.21)$$

since $dx = rd\varphi$ where r is the radius of the earth.

To retain a precision of 0.01 mgal, in middle latitudes, relative north-south distance must be accurate to roughly 10m (Nettleton, 1976).

3.6. DATA PROCESSING

3.6.1. Gridding

A grid is a rectangular region comprised of evenly spaced rows and columns. The intersection of a row and column is a grid node. Gridding generates a Z value at each grid node by interpolating or extrapolating the data values (Surfer help manual). Minimum Curvature is widely used in the earth sciences. The interpolated surface generated by Minimum Curvature is analogous to a thin, linearly elastic plate passing through each of the data values with a minimum amount of bending. Minimum Curvature generates the smoothest possible surface while attempting to honor the data as closely as possible, however it is not an exact interpolator. This means that data are not always honored exactly.

3.6.2. Regional-residual separation

Because a Bouguer map shows horizontal differences in the acceleration of gravity, only horizontal changes in density produce anomalies. Purely vertical changes in density

produce the same effect everywhere and so no anomalies result. The gravity field is a superposition of anomalies resulting from density changes at various depths. The smoothness of anomalies is generally roughly proportional to the depth of the lateral density changes (Telford et al., 1990). Whereas it is possible for a distributed anomalous mass to give an anomaly that appears to originate from a more concentrated deeper mass, a concentrated mass cannot appear to originate deeper. The horizontal extent and smoothness of an anomaly is therefore usually a measure of the depth of the anomalous mass, and this property can be used to partially separate the effects of anomalous masses that lie within a depth zone of interest from the effects of both shallower and deeper masses. The effects of deep masses are called the regional and the gravity field after near surface noise and the regional have been removed is called the residual; it presumably represents effects of the intermediate zone of interest.

There are many techniques that can be used to accomplish the regional-residual anomaly separation (Telford et al., 1990). The simplest methods are manual techniques such as graphical smoothing where a simple smooth regional anomaly is subtracted from the observed gravity anomaly to obtain a residual anomaly (Figure 3.2). An advantage of the manual techniques is that the interpreter may have information on the lateral location of the source bodies and this information can be used to select a “correct” regional anomaly.

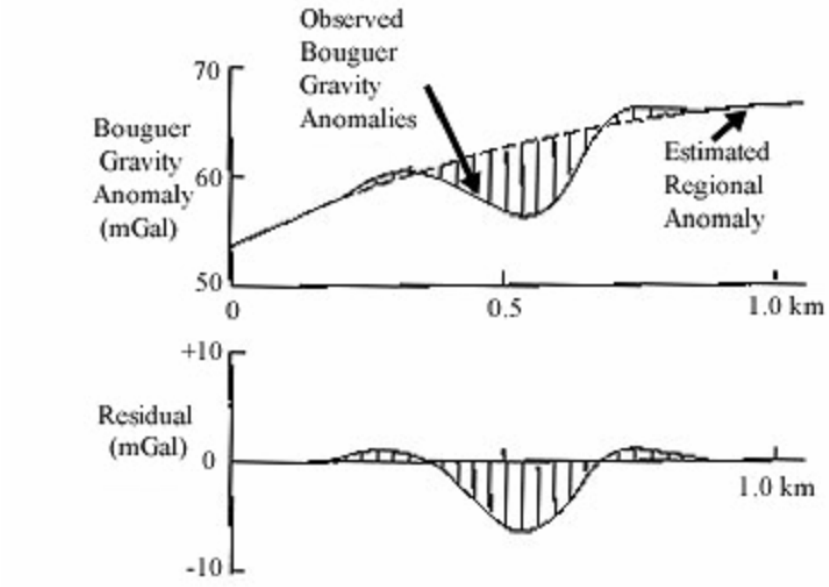

Figure 3.2 Example of a regional-residual gravity anomaly separation using graphical smoothing (adapted from Reynolds, 1998).

Most other regional-residual anomaly separation techniques involve mathematical operations using a computer. One problem with the mathematical techniques is that they do not accurately represent the “true” residual gravity anomaly due to a specific body. The most common mathematical technique is surface fitting. In this method the regional is represented by a low-order analytic surface. The parameters of the analytic surface are usually determined by a least-squares fit or some similar operation. How closely the surface fits the data depends on the order of the surface and the magnitude of the area being fitted. Nettleton (1976) illustrates orders of fit for a one-dimensional case. The regional surface is often that given by a polynomial or the low-order components of a 2D-Fourier surface. The selection of order is usually made by examination of trial fits of several different orders. Surface fitting is sometimes done to isolate and emphasize trends. The trend becomes more evident as the order increases up to some point. The residual for low order still contains appreciable regional trend and thus low orders are not very effective in separating the regional from the residual. Likewise, high-order surfaces are not effective because much of the sought-after anomaly is mixed with the regional in the surface fit.

3.7. Data Enhancement

Data enhancement techniques are used to increase the perceptibility of the gravity anomalies that might be related to bodies of interest. The most important techniques are derivative methods which are analytically calculated from a Bouguer gravity anomaly grid.

3.7.1. Second vertical Derivative methods

The second vertical derivative enhances near-surface effects at the expense of deeper anomalies. Second derivatives are a measure of curvature, and large curvatures are associated with shallow anomalies (Telford et al., 1990). The second vertical derivative can be obtained from the horizontal derivatives because the gravity field satisfies Laplace’s equation

$$\nabla^2 g = \frac{\partial^2 g}{\partial x^2} + \frac{\partial^2 g}{\partial y^2} + \frac{\partial^2 g}{\partial z^2} = 0 \qquad (3.22)$$

$$\frac{\partial^2 g}{\partial z^2} = -\left(\frac{\partial^2 g}{\partial x^2} + \frac{\partial^2 g}{\partial y^2}\right) \qquad (3.23)$$

Traditionally, the second vertical derivative has been the most commonly used derivative as the amplitude and width of a second vertical derivative is higher and narrower than the first vertical gradient and thus, supposedly easier to interpret. However, the second vertical derivative is more susceptible to data noise and errors, and topographic irregularities and should only be used for large-scale interpretations.

3.7.2. The Gradient operator

The gradient operator generates a grid of steepest slopes (i.e. the magnitude of the gradient) at any point on the surface (Surfer help manual). The gradient operator is reported as a number (rise over run) rather than in degrees, and the direction is opposite that of the slope. The gradient operator is zero for a horizontal surface, and approaches infinity as the slope approaches vertical.

The definition of the gradient yields the following equations:

$$\|\bar{g}\| = \sqrt{\left(\frac{\partial g}{\partial x}\right)^2 + \left(\frac{\partial g}{\partial y}\right)^2} \qquad (3.24)$$

3.7.3. Wavelength Filtering

Filtering can be done by transforming map data to a wavenumber-wavenumber domain using a two-dimensional Fourier transform removing certain wavenumber components and then doing an inverse transformation to reconstitute the map, but with certain wavelengths removed (Telford et al., 1990). Usually the small wavenumbers of the regional are removed, hence the wavenumber components involved in the inverse transform are the large ones which correspond to the short wavelengths of the residual. Wavenumber filtering encounters the problem that wavenumber spectra of most features are broadband, so spectra of features at different depths overlap and consequently the features cannot be separated completely by filtering.

3.8. THEORY OF EULER DECONVOLUTION

The Euler deconvolution is a method for estimating the depth of the source of a potential field anomaly. This technique is based on Euler's equation of homogeneity which defines the structural index corresponding to the homogeneity order of the source (Bourlon, ___). Assuming the type of source we can deduce its depth. A function *f(x,y,z)* is homogeneous with degree *n* if $f(ax,ay,az)=a^n f(x,y,z)$. This relation is equivalent to Euler's equation:

$$r \cdot \nabla f = nf \qquad (3.25)$$

Where r is the position vector (x,y,z). When f is a potential field, the exponent n depends on the source and the type of field. It is related to the structural index or attenuation rate N, by $N=-n$ for gravity and $N=-(n+1)$ for magnetics. As the potential fields of isolated homogenous sources are functions of the derivatives of $1/|r|$, they satisfy Euler's equation with their own characteristic integer value n. For the potential field f due to a single homogeneous source located (x_0,y_o,z_0) and that the observation location is(x,y,z), we can must determine the unknowns x_0,y_0,z_0 and n from the field measured on the plane z=0. We obtain as many equations as required for various locations. The gradients may be measured or computed. Standard algorithms generally assume a value of structural index in order to determine the location of the source (x_0,y_o,z_0). When the source is not a point source, this position locates a point between the top of the source and its center of mass. In case of gravity field, we find that: n=-2 for a sphere of uniform density (point mass); n=-1 for an infinite horizontal cylinder (line mass); n=0 for a step.

The homogeneity order is not necessarily an integer, the order of the gravity field of a thin sheet varies with its vertical dimension from -0.625 if it is infinite to -1(infinite line case). Since the Euler deconvolution method requires the neumerical evaluation of horizontal and vertical derivatives from the data, this method is very sensible to noise.

3.9. GRAVITY DATA MODELING

Gravity modeling is usually the final step in gravity interpretation and involves trying to determine the density, depth and geometry of one or more subsurface bodies. The modeling procedure commonly involves using a residual gravity anomaly. There are many

different techniques available to perform the modeling procedure and they can be broken down into three main categories: analytical solutions due to simple geometries, forward modeling using 2-(two-dimensional), 2.5- (two and one-half dimensional) and 3-D (three-dimensional) irregularly shaped bodies, and inverse modeling using 2-, 2.5- and 3-D irregularly shaped bodies. Most of these techniques involve iterative modeling, where the gravitational field due to the model is calculated and compared to the observed or residual gravity anomalies. If the calculated values do not match the observed anomalies, the model is changed and the procedure is performed again until the match between the calculated values and the observed anomalies is deemed close enough. Before the advent of computers, solutions to simple geometries (e.g., spheres, cylinders, prisms, thin sheets) were used to approximate subsurface mass distributions using residual gravity anomalies (Telford et al., 1990). What are more commonly used are simplifications of the analytical solutions to obtain an approximation of a body's depth. These simplifications are termed depth or half-width rules because they are based on the horizontal distance ($x_{1/2}$) from the maximum anomaly value to one-half of that anomaly value. The half-width formula for a sphere, which is used to determine the depth to the center of the sphere is:

$$Z=1.3\ X_{1/2} \tag{3.26}$$

Half-width rules are used in the field to determine a "quick" approximation to the depth of a given source. The most common technique in gravity modeling is computer forward modeling of polygonally-shaped, multiple 2- and 2.5-D bodies along profiles of data. The difference between 2- and 2.5-D is that for 2.5-D bodies, the cross-sectional shape extends out a finite distance (called strike lengths) in both directions perpendicular to the profile. 2- and 2.5-D models can be used to determine the lateral position and offsets of shallow faults, the thickness of the soil layer and the bedrock topography (Hinze, 1990). The final method of gravity interpretation is inverse modeling where given a set of observed data and a general starting model, a computer algorithm will determine a set of parameters (body geometry and density) that best fit the observed data. Along with determining a model, the algorithm may determine how well that model fits the data and a range of models that equally fit the given observed data.

CHAPTER FOUR

4. DATA PROCESSING

4.1. Introduction

The data used for this project was obtained from the Ethiopian Institute of Geological Surveys (EIGS). The gravity observation points lie between latitudes 7^0-8^0N and longitudes 38^0-39^0E (Figure 4.1). These points are distributed along seasonal and cross-country roads and off road transects. A total of 1200 gravity observation points were used in this study with an average spacing of 1km between consecutive stations. The gravity measurement for most of the stations was made with La Coste and Romberg (model G871) gravimeter and instruments used for measuring elevation are mainly hand held GPS and altimeters. All the gravity stations are tied to the International Gravity Standardization Net 1971 (IGSN71) and the observed absolute gravity values are corrected for the effect of elevation, the Bouguer effect of masses including the terrain variation effects. The reduction density used is the mean crustal density 2.67 gm/cm^3 and anomalies were calculated using the Geodetic Reference System of 1967 (GRS67).

Other tasks performed in this project include gridding, regional-residual separation, filtering, and modeling. These are described below:

4.2. Data Gridding

The reduced gravity data arranged in spreadsheet was imported into Surfer surface mapping software for processing. Processing started with gridding which averages nearby observation points to give a uniform distribution of grid node values, the gridding method applied for this purpose is minimum curvature. There are a total of 84 rows and 100columns and the spacing between grid nodes is 1300m.

4.3. Regional-Residual separation

Before interpretation commences, it is a common practice to remove the regional field from the anomaly map. This procedure, as discussed in the theoretical part, can be performed in different ways. One of such methods adopted here is surface fitting using a second order polynomial. The second order polynomial resembles the broad regional field of deep seated bodies.

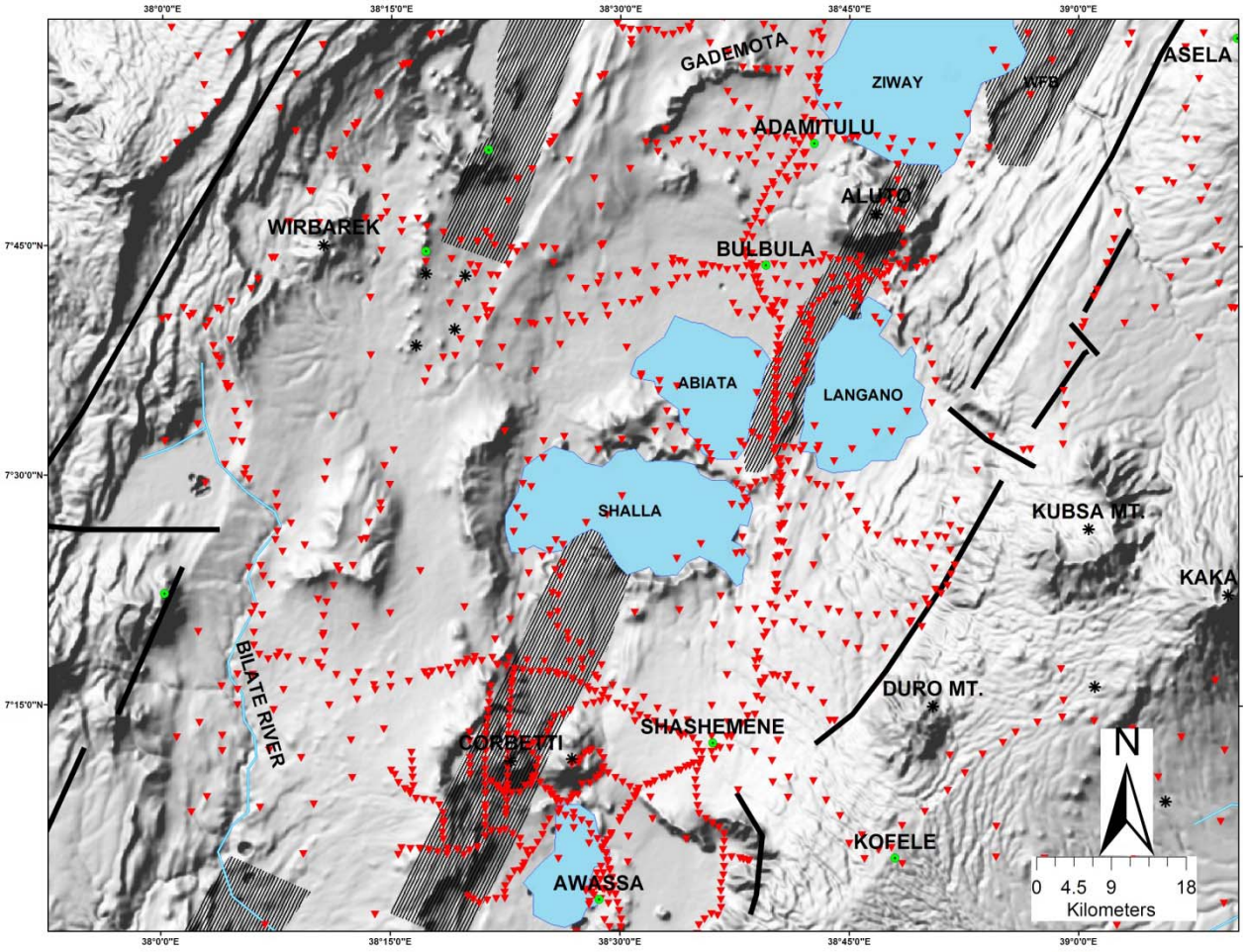

Figure 4.1 Gravity observation points overlaid on a 90m resolution shaded relief DEM. Gravity observation points are shown as Red inverted triangles, Dark strips and lines mainly trending NE represent Fault belts and border faults respectively.

4.4. Data filtering

Filtering was done using Surfer with the filter coefficients imported from Matlab7, filter design was carried out using the Signal Processing toolbox in Matlab7. The design involves specifying type of design method, frequency cutoffs, order and other options in the Filter design and analysis user interface. The designed filter can be viewed in different domains and repairs can be made using available editing options, when the design process

is completed the filter coefficients can be exported in different formats for application. In this project, a band pass filter was designed to remove effects of noise due to data quality, shallow depth anomalies with rapid wavelengths and anomaly responses deeper than the upper crust. The designed filter will enhance the response of the upper crust especially anomaly wavelengths in the top 10 kms. A finite impulse response Gaussian window with order 21 was used for this purpose. The cutoff frequencies were specified using the relation of depth and anomaly wavelength for three dimensional bodies obtained from the work of Radwan J. El-Kelani (2007). Accordingly, the wavelength between 6,000-30,000m with corresponding spatial frequency 0.000209-0.001047 Hz was used for modeling the upper 10 kms. The choice of filter order was based on finding a manageable matrix size searched through successive increment of order, the 21 order filter with the pass bands defined near the cutoff limits and stop bands attenuated to an acceptable degree was chosen as appropriate (Figure 4.2). The attenuation at cutoff frequencies is fixed to 6 dB and the highest frequency which is the same as the Nyquist frequency was taken as 0.00241Hz.

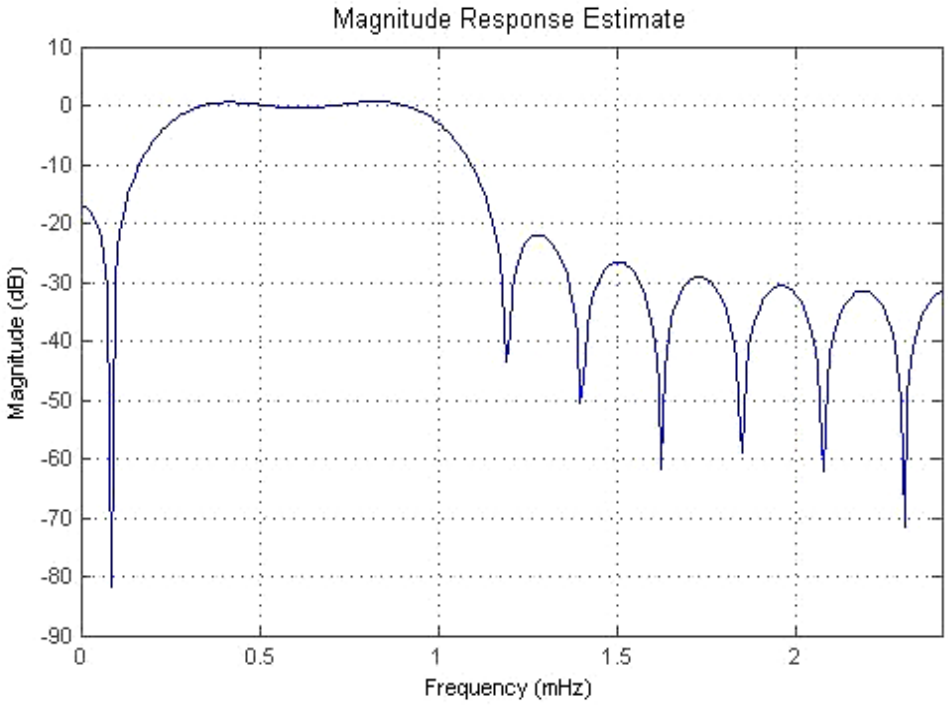

Figure 4.2 The finite impulse response Band pass filter applied to the gravity data. The filter is designed using Gaussian method to remove wavelength out of the range 6,000-30,000m.

4.5. Application of Euler Deconvolution

Euler deconvolution is an important tool for determining depth of contact and the method is applied here with this intent. The software Euler 1.15 works with profile data in this case extracted using Surfer in ASCII format. It will immediately calculate the vertical and horizontal gradients which are inputs for further calculations. Processing window requires defining structural index, window size, whether to use or not the vertical gradient in the calculation and other options. The result displays a trend line indicated by points which refer to geological contacts. For the modeled profile in this project, structural index 2, corresponding to a spherical source was chosen and the window size 14 which shows a good pattern of clustering around anomaly sources was chosen. In addition, the vertical derivative of the field was used because the results obtained using the observed gravity field show no definite pattern.

4.6. Gravity data Modeling

Data modeling was done with Grav 2dc. The software calculates the gravitational anomaly over up to fifty 2.5D bodies using a Talwani type algorithm. It allows the use of inversion, wherein mathematical techniques are used to modify the shape and other attributes of the model to improve the fit of the calculated curves to the observed data. The inversion uses ridge-regression and singular value decomposition. The drawback of using the program is that it is made to invert simple bodies and can only invert a body at a time. All edititng of the model is done in a user-friendly way.

In this project the software is used for forward modeling the initial model to compare the calculated response of the body with the observed data. The initial model for this project was constructed taking into consideration the regional geologic setup, the EAGLE Seismic refraction survey results, borehole data from the Aluto caldera and the work of Mammo, 2004 where surface waves were studied and showed the presence of the Mesozoic sequence.

The gravity point observations are sliced using Surfer software and imported in an ASCII format into the program. The initial model can be entered into the program either by drawing the expected density bodies or by entering directly the corners of the bodies using ASCII format files. The initial model is then progressively changed so that the observed gravity field matches the response of the forward modeled bodies. Successive improvement to the model is achieved through manual adjustment the body corners.

CHAPTER FIVE

DISCUSSION

5.1 The complete Bouguer gravity anomaly

The complete Bouguer gravity anomaly map is characterized by negative anomalies ranging from -250mGal to -150mGal. The map shows different anomaly patterns and can be broadly classified into regions with relative positive anomalies aligned in the direction of the rift and relative negative anomalies aligned transverse to the rift axis (Figure 5.1).

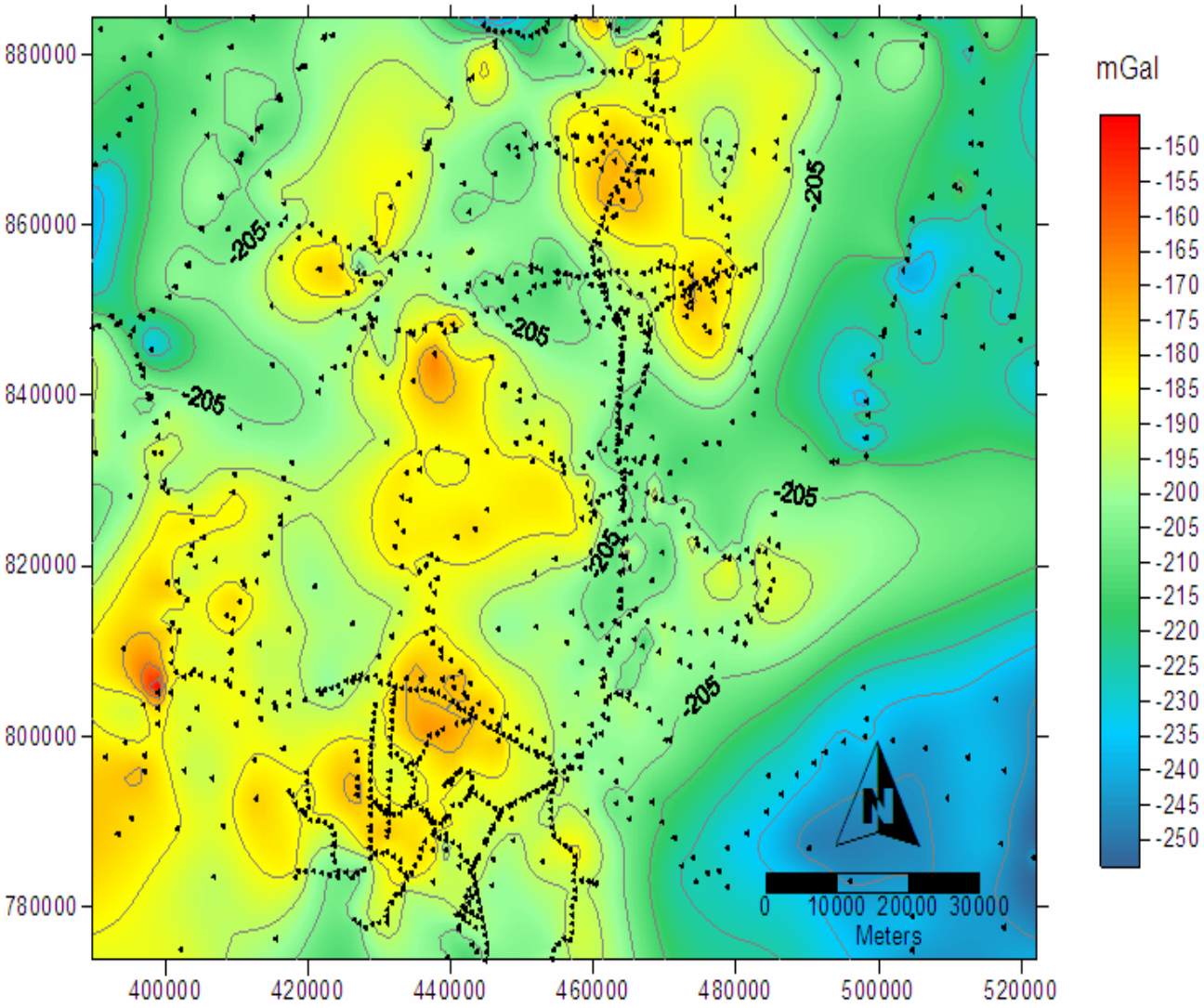

Figure 5.1 Complete Bouguer anomaly of the study area with 5mGal contour interval. Dark dots indicate locations of gravity observation points, UTM coordinate system is used.

The positive anomalies are represented by near circular patches bounded by intermediate anomalies and increasing in gradient towards a random point inside the bounded regions. The patches also show broadening in the south west direction. The peak anomalies (> -160mGal) are observed at few points distributed in the rift floor. On the other hand, the lowest gravity anomalies (< -205mGal) are observed to the south east and north east of the study area and in small proportion to the North West. These gentle anomalies are located at the plateaus separated by the boarder faults which are represented by steep gradients and straight contours. One reason for the relative decrease in magnitude of the Bouguer anomaly at the plateaus is a deeper Moho boundary. Mahatsente et al., 1999 characterized the crust in the central MER as anomalously thick under the plateaus ranging from 38 to

51km beneath the southeastern plateau, whereas the moho depth is relatively shallow (39-43km) under the western plateau.

The Bouguer anomaly contours overlain on the color coded Digital Elevation Model (DEM) map shows the relationship between elevation and complete Bouguer gravity anomaly (Figure 5.2). The trend of the topography shows a decrease in elevation towards the rift floor marked by the blue color, whereas topographic highs are observed towards the North West and South East corners of the map marked by warmer colors yellow and red. The Bouguer anomaly generally increases towards the rift floor with a pattern different from the decreasing pattern in elevation. This can be seen to the south west of the study area where positive Bouguer anomaly contours are found at higher elevation. Similarly, anomalies of the same order are found lying side by side at different elevations indicating the poor correlation between elevation and the Bouguer anomaly. Other evidences for the poor correlation can be observed at the border faults where the topography is represented as a high gradient slope but as can be seen in the north east and south west ends of the map concentric high amplitude Bouguer anomaly contours are observed. The anomaly contours towards the North West are still other evidences which show elongation in the direction transverse to the rift border faults towards the direction of positive gradient of elevation.

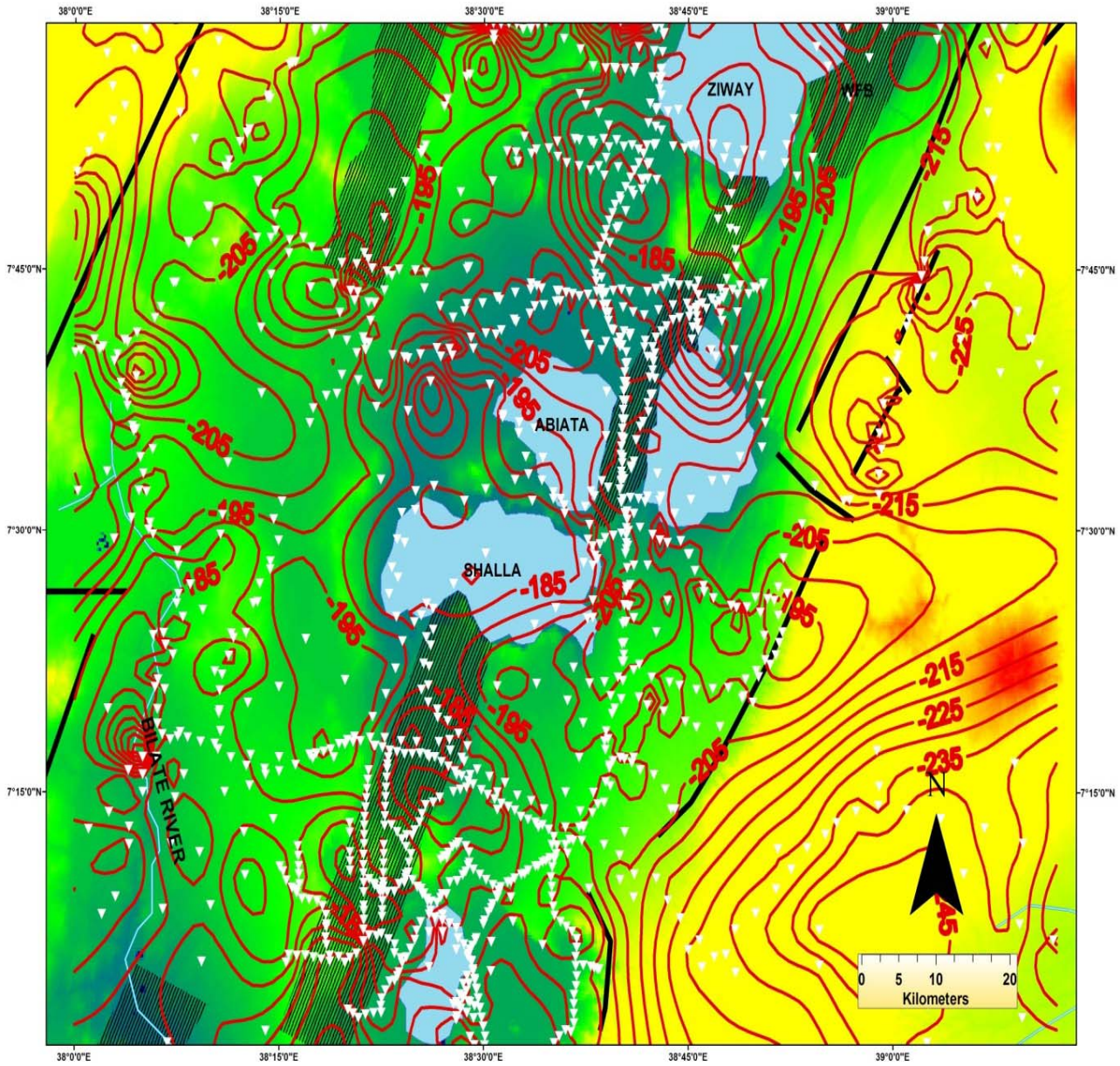

Figure 5.2 Complete Bouguer anomaly contours of the study area overlain in red (5 mgal contour interval) on a 90m resolution DEM where warmer colors indicate higher elevations and cooler colors indicate low elevations. Dark strips and lines mainly trending NE represents Fault belts and border faults respectively. Inverted triangles represent gravity observation points.

5.2. The regional Bouguer gravity anomaly

The regional field separated using polynomial surface fitting technique shows a broad negative anomaly and a superimposed positive anomaly disturbing the gentle gradient (Figure 5.3). The gravity values range between -265mgal and -185mgal. In the work of Tesema and Antoine (2004) a brief explanation is given about the broad gravity minimum

that coincides with the topographic relief of the plateau; it is suggested to be the result of a lithosphere eroded by an upwelling asthenosphere. In line with this, Ebinger et al., (1989) in Tesema and Antoine (2004) suggested that part of the East African topographic relief is dynamically supported by convective processes in the upper mantle and hence the upward buoyant thermal loading acting from the upper mantle is responsible for isostatic compensation of the anomalous topographic relief. An anomalous upper mantle is also indicated in a global seismic tomographic model (Grand et al., 1997 in Tesema and Antoine, 2004) suggesting that the East African plateau is underlain by anomalously low velocity upper mantle. In conclusion Tesema and Antoine, 2004 attribute these broad low gravity and velocity zone to an anomalous geotherm within the lithosphere. On the other hand, the superimposed positive anomaly is due to high density basic intrusions or a magma chamber in the crust.

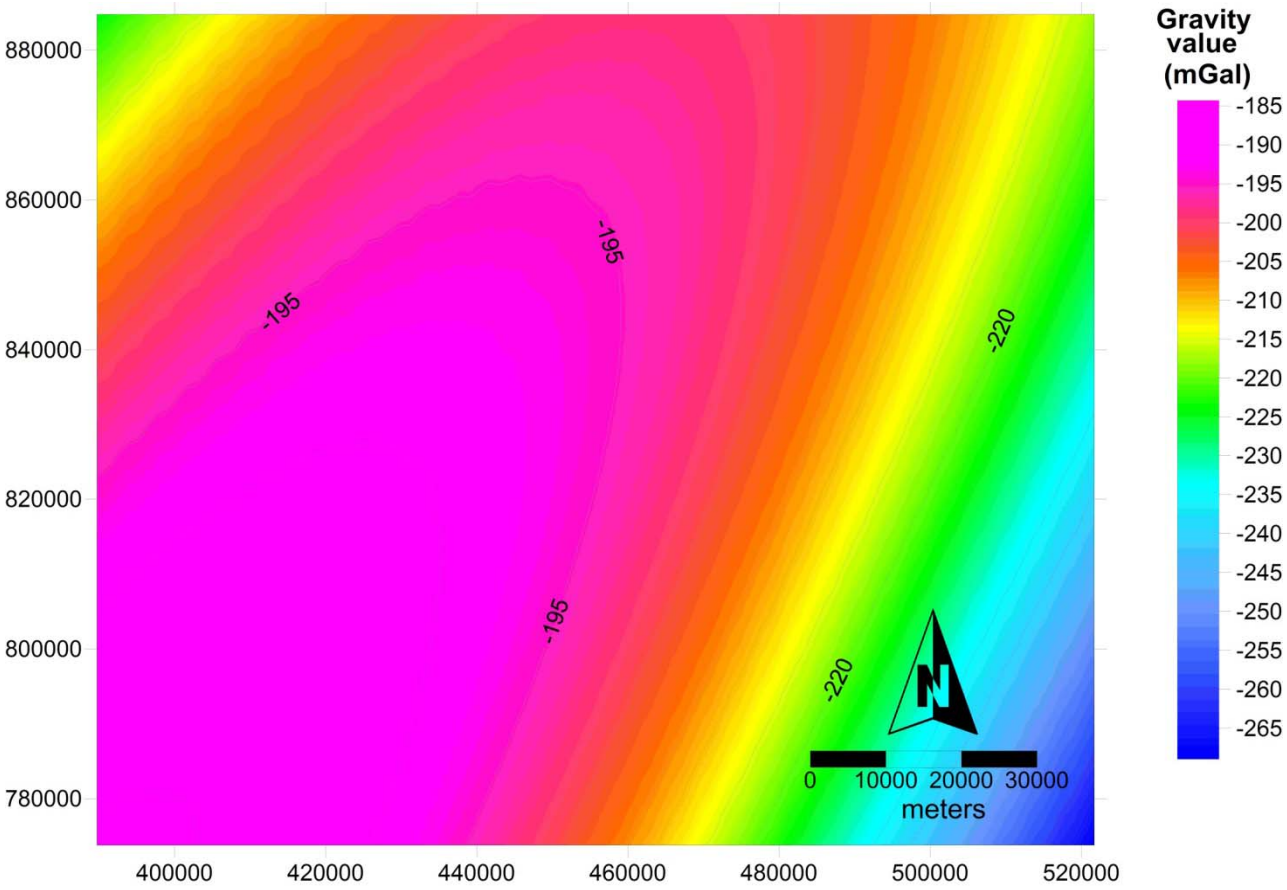

Figure 5.3 Regional Bouguer gravity anomaly map of the study area with contour interval 5mgals, UTM coordinate system is used.

5.3 The Residual Bouguer gravity anomaly

The Geological map overlain on a residual Bouguer anomaly map of the study area is a good way of interpreting the relations between gravity anomalies and geology. In this section geologic phenomenon is discussed in relation to the residual anomaly map.

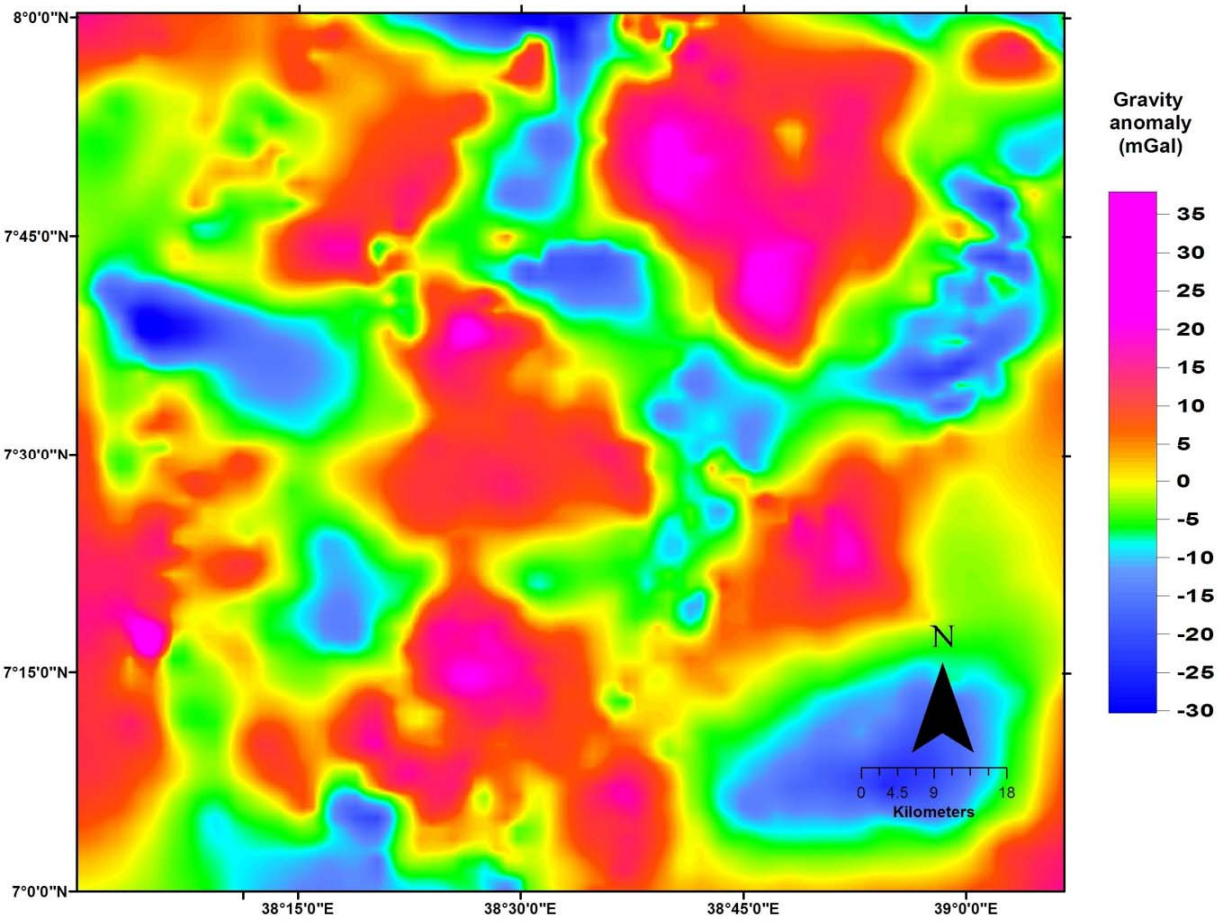

Figure 5.4 Residual Bouguer anomaly map of the study area with a contour interval of 5mGal.

In the study area the maximum anomaly observed (~15mGal) is in places such as inside the Gademota caldera, between Aluto and Lake Langano, over the lacustrine deposits to the west of Lake Abiata, on the eastern border faults to the west of Mt. Kusba and around the Corbetti caldera. These distributed features have circular contours. Anomalies due to tectonic activities like faults are represented by near straight contours (Figure 5.5) and Caldera rims show contour patterns that resemble the rims.

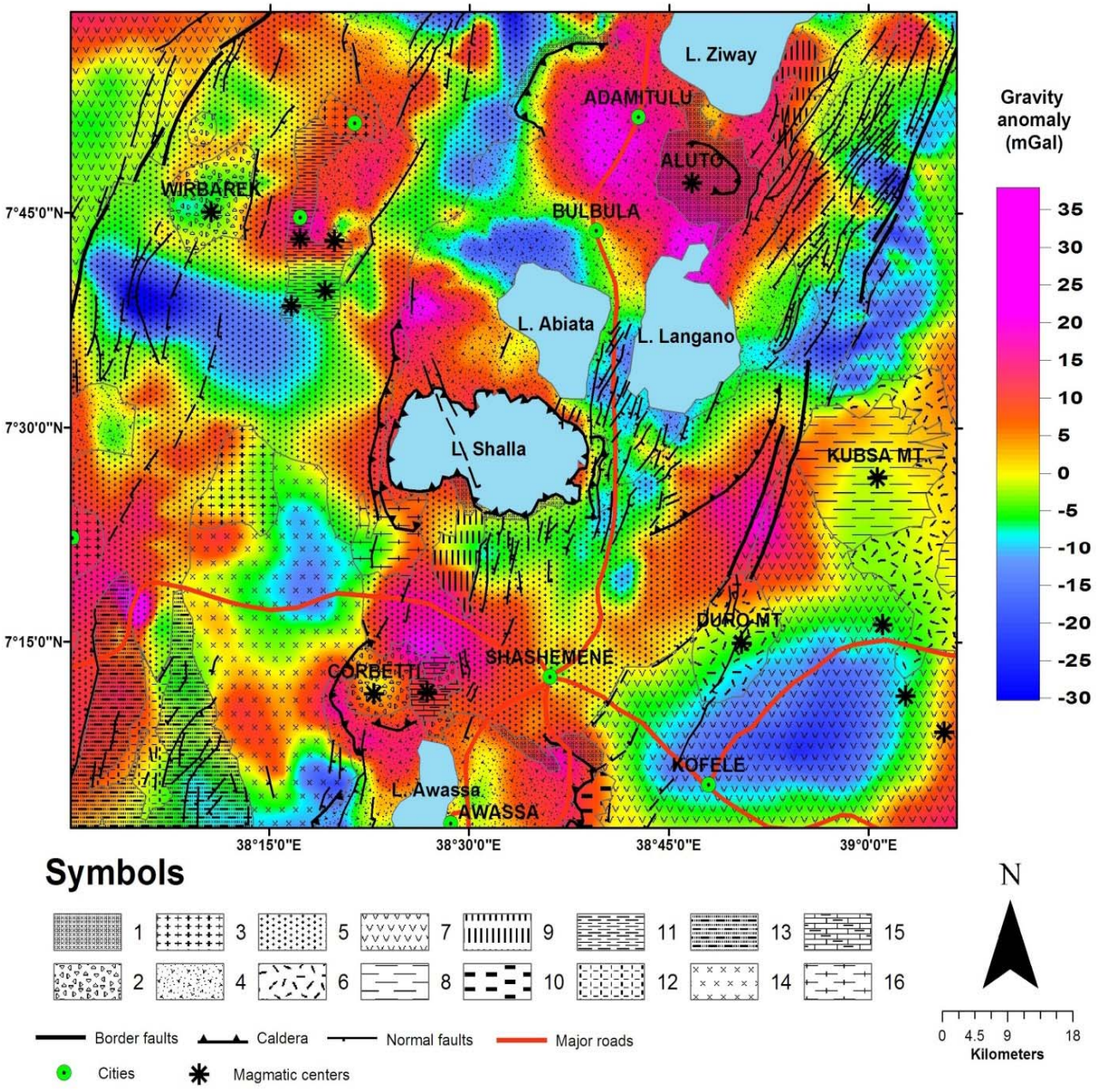

1-Rhyolitic and trachytic lava flows, 2- Pumice and unwelded tuffs, 3- Peralkaline silicics undifferentiated, 4- Lacustrine sediments, silts, clays, diatomites, volcanoclastics and tuffs, 5- Ignimbrites, Tuffs, waterlain Pyroclastics, occasional lacustrine beds, 6- Trachytes, trachybasalts, peralkaline rhyolitic ignimbrites, 7- Nazret Group and Dino formation, 8- Alkaline basalts, 9- Pleistocene basalts, 10- Alkaline basalts, trachytes and peralkaline rhyolitic ignimbrites undifferentiated, 11- Recent and subrecent basalt flows and cones, 12- Ignimbrites, alkaline basalts, trachytes and peralkaline rhyolitic ignimbrites undifferentiated, 13- Volcano-sedimentary rocks: lacustrine, predominantly volcanoclastic sediments, tuffs 14- Coarse unwelded pumiceous pyroclastics, 15- Obsidian and pitchstones, 16- Basaltic hyaloclastites,

Figure 5.5 Relationship between the residual Bouguer anomaly map and geology of the study area. A geological map, complied by Kazmin and Berhe, 1981, overlain on a Bouguer anomaly map with contour interval 5mGal.

To the south of the study area, the anomaly over the Corbetti caldera shows a complex structure. Its exposed southern rim is represented by a similar pattern Bouguer anomaly contour of 10 mgal and its immediate center to the north shows intermediate positive anomaly over the pyroclastic caldera floor formation. Farther to the northeast a positive anomaly having identical anomaly pattern and magnitude with the Gademota but with broader circular contours and less steep gradient is located. This can be explanied as the response of a Rhyolite center within the active Wonji fault belt. In the gradient map (Figure 5.6) the picture is much more simplified where a large body encompassing Corbetti and the nearby high amplitude positive anomaly is observed suggesting a single source. A positive anomaly is also observed west of Lake Awassa having slightly higher magnitude and width than the anomaly over Corbetti corresponding to the magma chamber beneath the caldera shown in the geological map.

The Bilate River is located near the western border faults flowing in the north-south direction following a fault line. The anomaly map shows a peak anomaly over the river at the intersection with the Shashemene-Sodo road. The shape of the contours and high amplitude suggest the presence of a dike. Furthermore, the gradient map (Figure 5.6) defines the fault line and shows the presence of other deeper intrusions along strike the fault. On the other hand the south eastern border faults are represented by straight contours aligned in the north east direction. This general trend of contours continues to the north eastern part of the study area which is a site of intense faulting representing the marginalized WFB. The pattern of these contours is disturbed in many cases by circular positive anomalies having different wavelengths. These features are results of fault related intrusion found at different depths as indicated by the variable wavelength contours.

In the Northern part of the study area the anomaly pattern shows distinct features where strong positive gravity anomalies with comparable magnitudes and circular contours exist inside the Gademota caldera, north of Lake Langano and on top of the lacustrine deposits to the west of Lake Abiata with their center a negative anomaly having elliptical to irregular geometry contours.

The surface geology shows poor correlation with the magnitude of the Bouguer anomaly with most of the sites covered by the lacustrine deposits. The Aluto is found nearby with the maximum anomaly over its center of 5mgals. A gradient map for the residual anomaly

filtered with a band pass filter using wavelength limits 3km and 30km reveals different patterns. Among these is the gradient observed around the Gademota caldera.

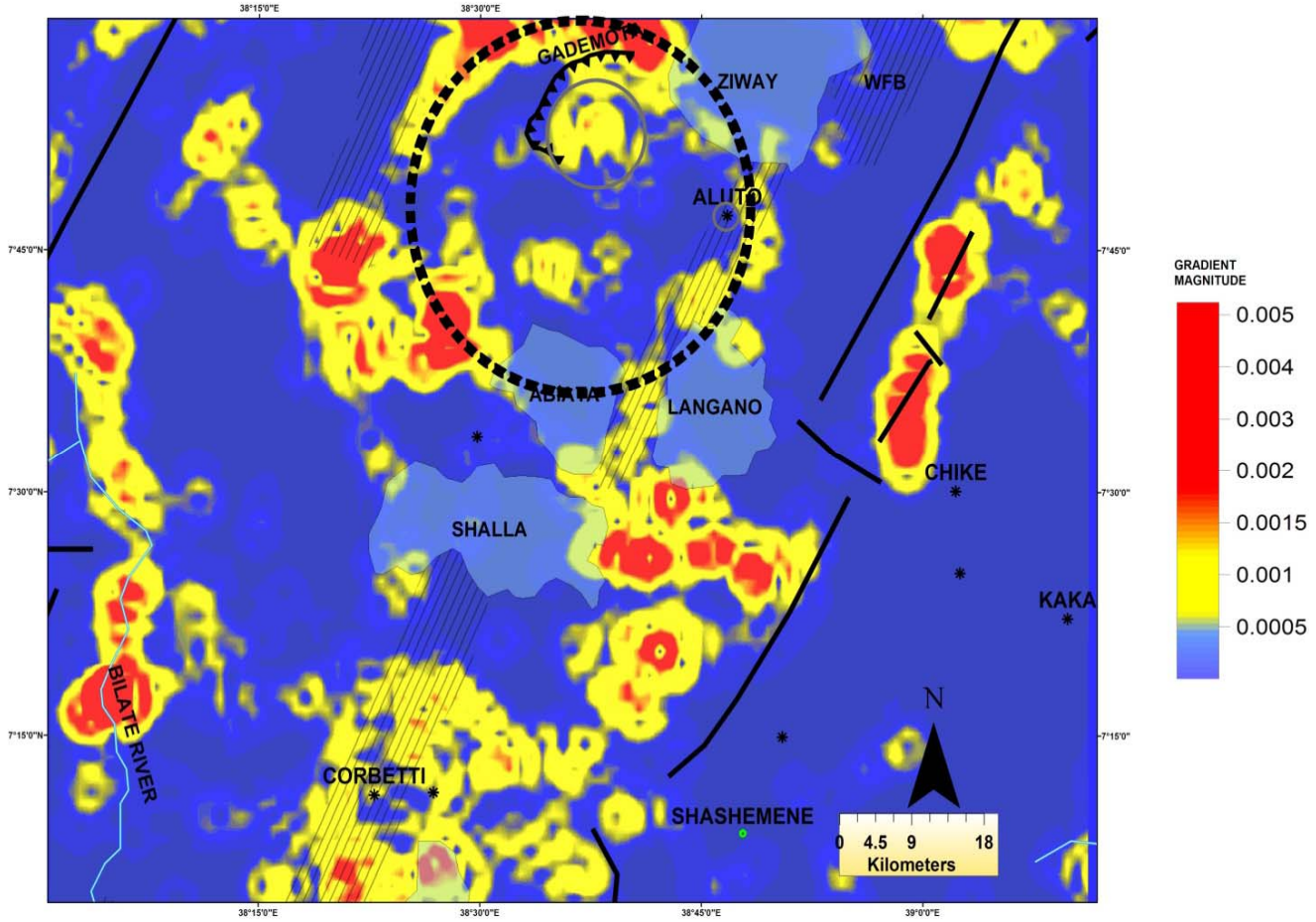

Figure 5.6 Gradient map of the filtered Bouguer gravity anomaly. A band pass filter with cut-off frequencies 0.000209Hz and 0.001047Hz is applied. Dashed line shows the proposed caldera rim and solid circles inside show the rims of the Gademota and Aluto caldera. Dark lines and strips represent the border faults and fault belts respectively; pointed stars refer to magmatic centers.

Previous works (Woldegebreal et. al., 1990 and references there in) described Gademota as an eroded western rim of a large (30-km diameter?) caldera with its eastern rim buried under younger rocks. However, as can be seen in Figure 5.6, it is possible to fit a circle on the steep gradients around Gademota moving further behind Aluto and through the Lakes which discontinue the rim and back to Gademota. South west of this proposed rim a high gradient circular feature is represented in the surface geological map by lacustrine deposits; this is included to be part of a bigger diameter caldera. The floor of the proposed caldera shows uniform gradient distribution except at the Gademota and to the north of

Lake Abiata. A possible geologic model to explain thse observations is a large magma chamber which vacated after a series of volcanic eruptions and collapsed to give a caldera structure, estimated here to have a diameter of ~42kms, where subsequent magmatic activity continued to upwell near its rims resulting in the Gademota and Aluto calderas and in a number of intrusions having higher densities. The caldera was later filled with low density volcanic and sedimentary deposits. Supportive evidence of this proposed caldera rim is found in the work of Woldegabreal et.al., (1990) where the authors estimated a source of the stratigraphically and petrologically across rift correlatable voluminous crystal rich tuff. By taking into consideration the distribution, petrological and geochemical relationships the authors reasoned a source for this voluminous ash-flow tuff to be on the rift floor between Guraghe and Munesa. Further they attributed the absence of a caldera remnants, from which such an immense unit might have erupted to burial under subsequent eruptions and tectonic subsidence.

Anomalies over the lacustrine deposits and low density pyroclastic rocks lie in the range between -5mgal and 5mgal in the residual anomaly map. These gentle gradient features as seen in the gradient map (Figure 5.6) cover much of the area in the rift floor and the adjacent plateaus. The formations surrounding the lakes have shallow depths as can be seen from the contours of the residual anomaly and the depth of these formations increase near the western border faults which show an east west elongation. Other prominent feature in the study area is the patch of high gradient bodies south of Lakes Langano and Shalla. This feature is poorly defined in the residual anomaly map and is separate from the anomaly in the south. A magma chamber best describes its arrangement. The boundary faults to the west of mount Chike are still other prominent anomalies well represented in the gradient map and magma rising following weak zones is a probable cause. Other than this, due to minimum data coverage magmatic centers such as Kaka, Kusba and others in the study area show no response in the anomaly contours.

The filtered anomaly map (Figure 5.7) shows similarity in the general arrangement of anomalies with the residual anomaly map produced using surface fitting techniques, the main difference between the two being the width of the anomaly range. This map shows comparable positive anomalies lying in a narrow zone along the rift axis bounded by an intermediate and widespread anomaly range shown in yellow. The minimum anomaly magnitudes are observed at the plateaus and interspersed in the rift floor.

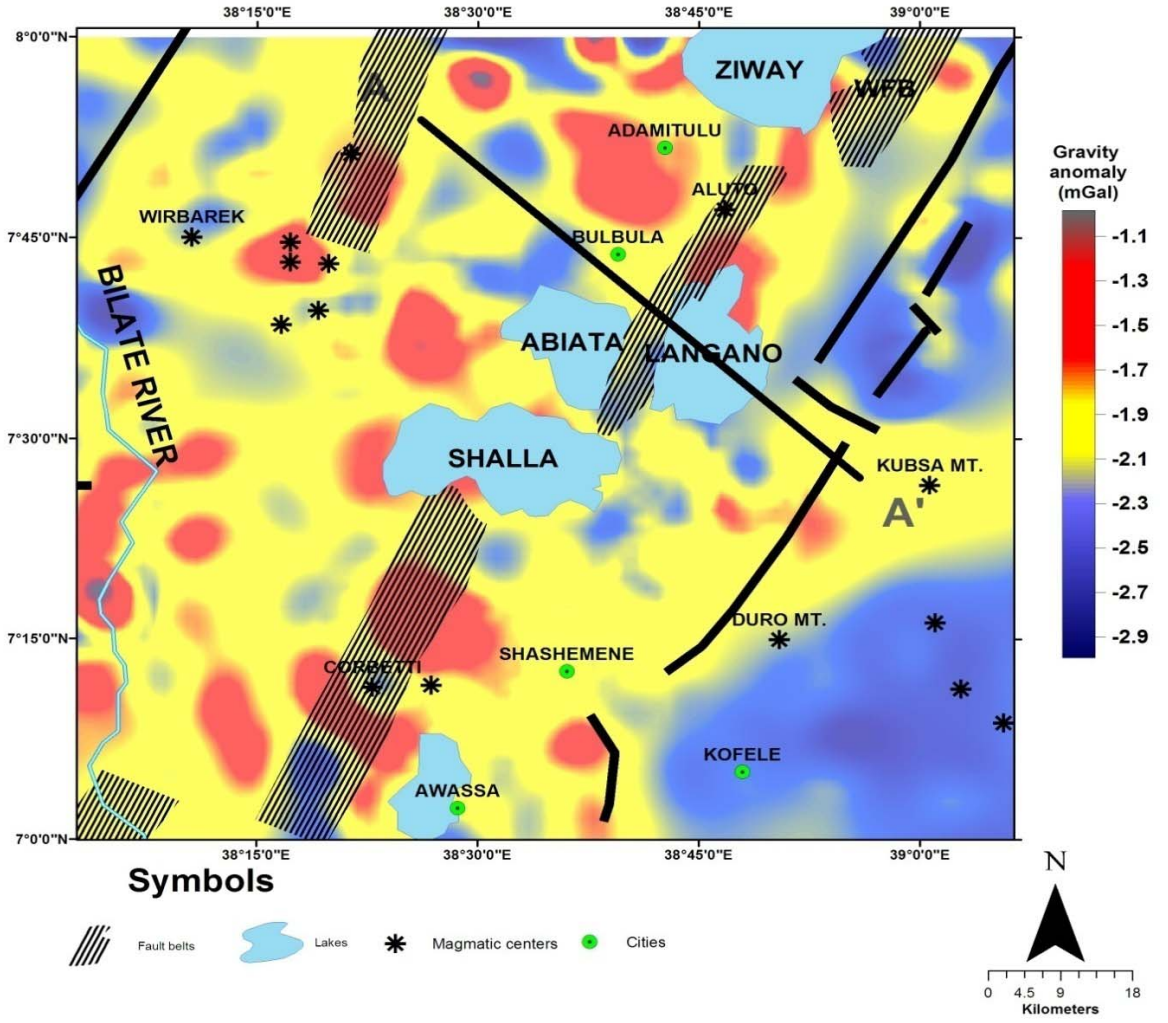

Figure 5.7 A band pass filtered anomaly map of the study area. A band pass filter with wavelength limits 6km and 30kms is applied to the complete Bouguer anomaly map to give this anomaly map. Line A-A' shows the model profile.

5.4 Interpretation of the gravity model

5.4.1 Results of Euler deconvolution

The Euler deconvolution shows different clustering patterns close to a layer boundary at a depth of ~3000m when the structural index is two. The clusters represented by different letters in figure 5.8 are the results of short wavelength anomalies where Letter "A" represents the position of the vertical contact that exists in the basement due to lateral in homogeneity. Letter "B" represents the position and depth of a shallow vertical contact at a depth of ~700m; it is modeled as a fault. Letter "C" on the other hand shows a typical

clustering pattern over the top of a dike at a depth ~3000m. Letters “D” and “E” show similar orientation and are interpreted to be fault contacts on top of the basement whose contact with the basement reaches ~3500m. Due to the noise in the data a shallow horizontal contact is observed near the right end of the profile, this has not been considered in the model.

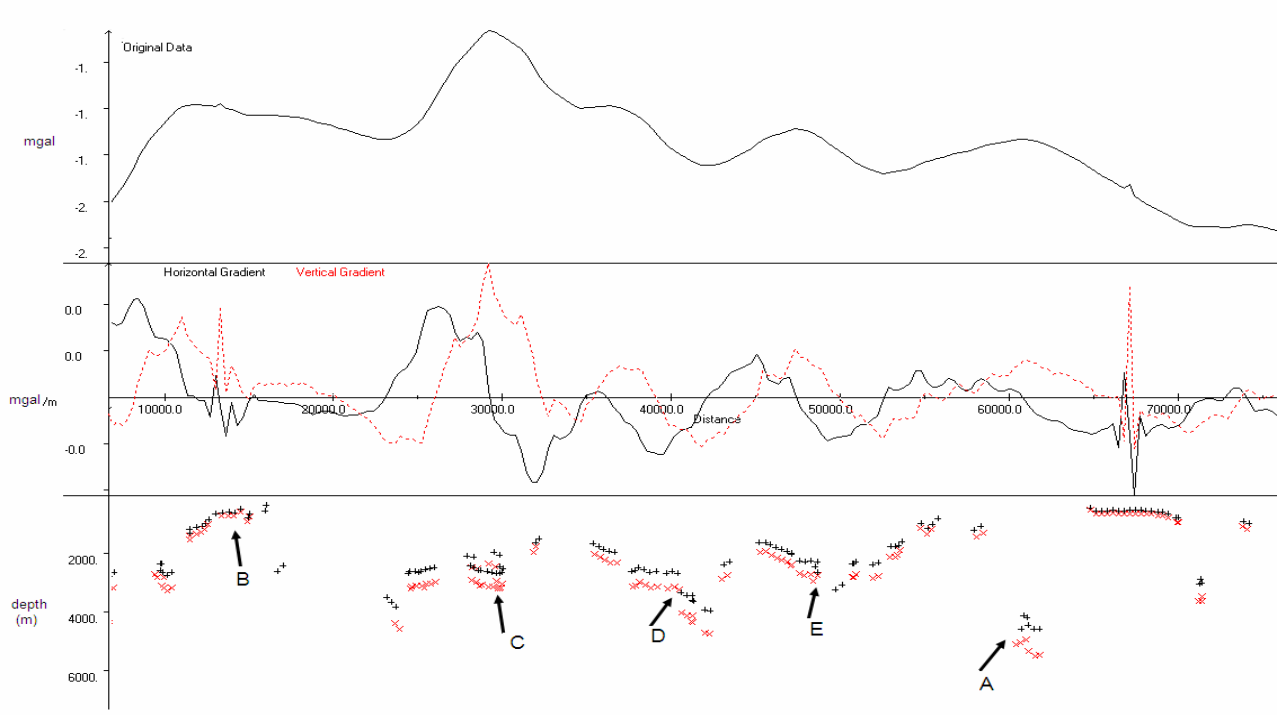

Figure 5.8 Euler deconvolution results for the profile A-A’. The Euler deconvolution was calculated using window size 14 and structural indices 2 represented by dark "+” sign, structural index 2.5 represented by red “x”.

5.4.2 Density constraints

Constraining density estimates of rock units in the upper crust of the study area have been determined previously. These density sources give estimates as follows:

1) The EAGLE controlled-source experiment determined a velocity model along the axis of the Main Ethiopian Rift (Keranen and Klemperer, 2007). In this model the upper 10 km crust of the study area is represented by three velocity layers; 3km/sec for the top ~300m loose volcanic and sedimentary products, 5km/sec for the ~2 km

thick formation overlying the basement and an average 6.01km/sec for the basement, these velocities refer to densities 2.22 gm/cm^3, 2.56 gm/cm^3 and 2.77 gm/cm^3 respectively using the Nafe-Drake (1957) relation.

2) The result of a seismic refraction survey in south western Afar (Makris and Ginzburg, 1987 in Mahatsente et al. 1999) has given different layer velocities, the corresponding densities estimated using Nafe-Drake (1957) relations are 2.5 gm/cm^3 for sediments; 2.7-2.78 gm/cm^3 for the upper crust and 2.9 gm/cm^3 for the lower crust.

3) Belaineh (1995) analyzed densities of 20 core samples from deep well LA-3 and 3 surface samples and determined densities for basalts, 2.57-2.67 gm/cm^3; silicic breccias and weakly welded tuff, 1.97-1.99 gm/cm^3; the Aluto rhyolite lava, 2.4-2.58 gm/cm^3 and for the Teritary crystalline Ignimbrites, 2.39-2.55 gm/cm^3.

In general the densities from seismic velocities show similar results where the basement is represented in both studies by density 2.7-2.78 gm/cm^3 and the overlying formation lamped in the case of Makris and Ginzburg, 1987 in Mahatsente et al.,1999 is refined to two layers in the EAGLE experiment. The result of Belaineh (1995) shows an average density of 2.39 gm/cm^3 for the whole section, this cannot be representative density of the top ~2kms because of the lateral in homogeneity that exists in the volcanic rocks.

5.4.3 Gravity modeling results and interpretations

The profile chosen for modeling (Figure 5.7) contains different anomaly wavelengths. The long wavelength anomaly has approximately the same width as the profile and superposed on this wavelength are short wavelength anomalies of local effects.

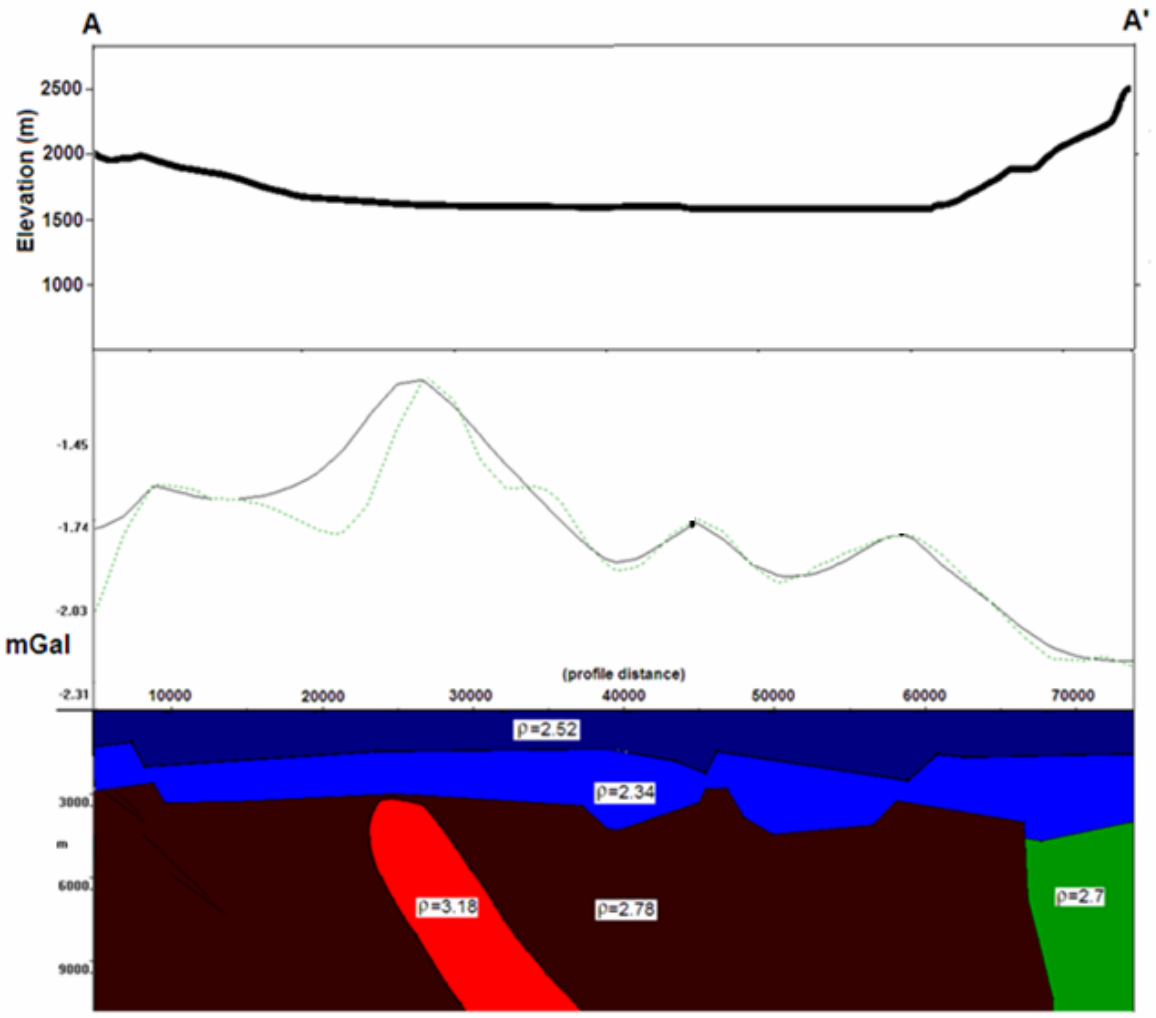

Figure 5.9 Gravity model for the profile A-A'. The dark line represents the calculated anomaly and the green dashed line represents the observed gravity values.

The forward model shows three horizontal density layers with densities 2.52gm/cm^3 on top, 2.34 gm/cm^3 in the middle and the lower layer represented by densities 2.78 gm/cm^3 and 2.7 gm/cm^3. The top layer represents the volcanic rocks and quaternary sediments and its thickness varies in the range between 1400 m and 2500 m. The maximum thickness is found near the Wonji fault belt towards the right end of the profile line, the thickness decreases away from this zone to a range of 1200-1600m. The second layer having lower density is inferred to be the Mesozoic sequence underlying the volcanic rocks. The thickness of this layer is variable due to the intense faulting in the region. In parts of the profile less affected by faulting the thickness of the sequence lies in the range between 1000-2000m and the thickness is maximum in tectonic troughs which are results of an early phase tectonic activity in the region giving a basin type architecture which was later

filled by sediments during the Mesozoic era. Also, from the model a gradual increase in thickness towards the east of the profile is observed. The bottom layer represents the Precambrian basement which shows a lateral variation separated by a vertical contact. This variation can be attributed to difference in grade of metamorphism. The highest density in the model is due to a dike that has intercepted the Precambrian basement. Its density is indicative of a basaltic composition.

From earlier discussions about the model it can be shown that the structural setup of the area is represented by different phases of tectonic activity. The phases are defined by the relative age of faulting, which is interpreted based on the age of the youngest unit it displaces. Hence, three phases of faulting are recognized in the model. The first phase is related to the accretion of the Precambrian basement complex as inferred from the pervasive vertical contact between the 2.78 gm/cm^{3}and the 2.7 gm/cm^3. The second phase may or may not be contemporaneous with the first, but older than Mesozoic era resulted in the undulations of the basement. The third and recent tectonic activity took place during the quaternary where faults of variable throw cutting all the layers belong to this group.

CHAPTER SIX

CONCLUSIONS AND RECOMMENDATIONS

6.1 **Conclusions**

From the gravity data processing and modeling procedures two important results have been obtained:

1) The combined filtering and horizontal gradient methods have effectively outlined the boundaries of a buried caldera rim which has only been inferred in previous works. The result shows a large caldera (diameter~42km) lying in the rift axis and encircling the Gademota and Aluto.

2) Gravity data modeling has shown the presence of the Mesozoic sequence which is inferred to be the low density layer (2.3gm/cm^3) lying between the higher density volcanic rocks and the basement. The layer has a variable thickness resulting from basement undulations and a series of Cenozoic faulting. The model has been constrained by depth obtained from the Euler deconvolution and previous density observations.

6.2 **Recommendations**

-The results of this work can be further improved and refined with the use of more precise elevation surveying instruments and processing techniques.

-The variable depth to the Mesozoic sedimentary sequence implies that a drilling program guided with geophysical results will intercept the sequence at a shallower depth.

References

Belaineh, M., 1995, Some physical properties of core samples from well LA-3 and surrounding areas Aluto-Langano geothermal field, Ethiopia. SINET: Ethiop. J. Sci., 18, 149-157.

Bourlon, E., ____, Analysis of Gravity and Magnetic fields in the Canadian Shield using standard and wavelet based methods. PhD thesis. University of Quebec, Canada, pp.187.

Burger, H.P., 1992, Exploration geophysics of the shallow subsurface: Prentice-Hall Inc. pp. 489.

Grav2dc, V.2.10 for Microsoft windows (2003). School of Geosciences University of the Witwatersrand, Johannesburg, South Africa. www.cooperg@geosciences.witz.ac.za.

Hinze, W. J., 1990, The role of gravity and magnetic methods in engineering and environmental studies, in Ward, S.H., Ed., Geotechnical and environmental geophysics: 1, Society Exploration Geophysicists, 75-126.

Kearey, P., and Brooks, M., 1991, An Introduction to Geophysical Exploration: Blackwell Scientific Publications, pp.254.

Keranen. K., Klemperer., S.L., 2007. Discontinuous and Diachronous evolution of the Main Ethiopian Rift: Implications for development of continental rifts. Earth and planetary Science Letters 265, 96-111.

Korme, T., Chorowicz, J., Collet, B., Bonavia, F.F., 1997. Volcanic vents rooted on extension fractures and their geodynamic implications in the Ethiopian rift. Journal of volcanology and geothermal research 79, 205-222.

Mahatsente, R., Jentzsch, G., Jahr, T., 1999. Crustal structure of the Main Ethiopian Rift from gravity data: 3-Dimensional modeling. Tectonophysics 313, 363-382.

Matlab Version 7.0.0. (2004), The language of technical computing. The MathWorks, Inc.

Nafe, J.E. and Drake, C.L. 1957, Variation with depth in shallow and deep water marine sediments of porosity, density and the velocities of compressional and shear waves. Geophysics 22, 523-552.

Nettleton, L.L., 1976, Gravity and Magnetics in oil prospecting: Mc GRAW-HILL Book company, pp.464.

Radwan J. E., 2007, Interpretation of Gravity Data in the Jericho Area, Dead Sea Transform. The Islamic University Journal. Vol. 15, No. 2, pp. 21-39.

Reynolds, J.M., 1998, An introduction to applied and environmental geophysics: Wiley and Sons, pp.796.

Surfer Version 8.00 (2002), Surface mapping system. Golden Software, Inc., Colorado, U.S.A.

Tefere, M., Chernet, T., Haro, W., 1996. Explanation of the Geological map of Ethiopia Scale 1:2,000,000. Ethiopian institute of geological surveys. Bull. No.3.

Telford, W.M., Geldart, L.P., and Sheriff, R.E., 1990, Applied Geophysics, Cambridge Univ. Press, pp.796.

Tessema, A., Antoine, L.A.G., 2004. Processing and interpretation of the gravity field of the East African Rift: implication for crustal extension. Tectonophysics 394, 87-110.

WoldeGabriel. G., Aronson, J., Walter, R.C., 1990. Geology, geochronology and rift basin development in the central sector of the main Ethiopian rift. Geol. Soc. Amer. Bull. 102, 439-458.

DECLARATION

I DECLARE THAT THIS THESIS IS MY ORIGINAL WORK AND HAS NOT BEEN PREPARED FOR ANY DEGREE IN ANY UNIVERSITY, AND THAT ALL THE SOURCES OF MATERIALS USED FOR THE THESIS HAVE BEEN DULY ACKNOWLEDGED.

_____

MEBATSEYON SHAWEL

This thesis has been submitted for examination with my approval as university advisor.

_____

DR. TILAHUN MAMMO